UNIVERSIDADE FEDERAL DO PARANÁ

ISADORA DA SILVA ZANZARINI

IDENTIFICATION AND CHARACTERIZATION OF MAGNOLOL DERIVATIVES AS
SELECTIVE ABCG2 INHIBITORS AND DEVELOPMENT OF A SIMPLE AND LOW-
COST LED-BASED PHOTODYNAMIC THERAPY DEVICE FOR *IN VITRO* ASSAYS

IDENTIFICAÇÃO E CARACTERIZAÇÃO DE DERIVADOS DO MAGNOLOL COMO
INIBIDORES SELETIVOS DO TRANSPORTADOR ABCG2 E DESENVOLVIMENTO
DE UM EQUIPAMENTO SIMPLES, DE BAIXO CUSTO E A BASE DE LED PARA
REALIZAÇÃO DE ENSAIOS *IN VITRO* DE TERAPIA FOTODINÂMICA

CURITIBA

2022

ISADORA DA SILVA ZANZARINI

IDENTIFICATION AND CHARACTERIZATION OF MAGNOLOL DERIVATIVES AS SELECTIVE ABCG2 INHIBITORS AND DEVELOPMENT OF A SIMPLE AND LOW-COST LED-BASED PHOTODYNAMIC THERAPY DEVICE FOR *IN VITRO* ASSAYS

IDENTIFICAÇÃO E CARACTERIZAÇÃO DE DERIVADOS DO MAGNOLOL COMO INIBIDORES SELETIVOS DO TRANSPORTADOR ABCG2 E DESENVOLVIMENTO DE UM EQUIPAMENTO SIMPLES, DE BAIXO CUSTO E A BASE DE LED PARA REALIZAÇÃO DE ENSAIOS *IN VITRO* DE TERAPIA FOTODINÂMICA

CURITIBA

2022

FICHA CATALOGRÁFICA

TERMO DE APROVAÇÃO

MINISTÉRIO DA EDUCAÇÃO
SETOR DE CIÊNCIAS DA SAÚDE
UNIVERSIDADE FEDERAL DO PARANÁ
PRÓ-REITORIA DE PESQUISA E PÓS-GRADUAÇÃO
PROGRAMA DE PÓS-GRADUAÇÃO CIÊNCIAS
FARMACÊUTICAS - 40001016042P8

TERMO DE APROVAÇÃO

Os membros da Banca Examinadora designada pelo Colegiado do Programa de Pós-Graduação CIÊNCIAS FARMACÊUTICAS da Universidade Federal do Paraná foram convocados para realizar a arguição da tese de Doutorado de **ISADORA DA SILVA ZANZARINI** intitulada: **Identification and characterization of magnolol derivatives as selective ABCG2 inhibitors and development of a simple and low-cost LED-based photodynamic therapy device for in vitro assays**, sob orientação do Prof. Dr. GLAUCIO VALDAMERI, que após terem inquirido a aluna e realizada a avaliação do trabalho, são de parecer pela sua APROVAÇÃO no rito de defesa.

A outorga do título de doutora está sujeita à homologação pelo colegiado, ao atendimento de todas as indicações e correções solicitadas pela banca e ao pleno atendimento das demandas regimentais do Programa de Pós-Graduação.

CURITIBA, 16 de Dezembro de 2022.

GLAUCIO VALDAMERI
Presidente da Banca Examinadora

ALAN GUILHERME GONÇALVES
Avaliador Interno (UNIVERSIDADE FEDERAL DO PARANÁ)

MARC LE BORGNE
Avaliador Externo (UNIVERSITÉ CLAUDE BERNARD LYON 1)

AHCÈNE BOUMENDJEL
Avaliador Externo (UNIVERSITé GRENOBLE ALPES)

RESUMO

O câncer é uma das doenças de maior índice mundial de mortalidade e o surgimento de resistência à quimioterapia convencional agrava ainda mais este problema. São descritos diversos mecanismos relacionados à resistência à múltiplas drogas (MDR) em câncer, porém a superexpressão de transportadores ABC é considerada a principal causa deste quadro clínico. O genoma humano codifica 48 transportadores ABC, dentre os quais 3 destacam-se quanto aos seus respectivos envolvimentos no fenótipo de MDR: Glicoproteína-P (P-gp ou MDR1), multidrug resistance associated protein-1 (MRP1) e breast cancer resistence protein (BCRP ou ABCG2). Estes três transportadores são capazes de reconhecer e promover o efluxo de uma ampla gama de agentes antineoplásicos, quimicamente não relacionáveis entre si. Por esta razão, novos compostos vêm sendo estudados para inibir a atividade de transporte mediada por essas proteínas. Apesar de ser um dos três transportadores ABC com maiores índices de envolvimento na MDR, o ABCG2 ainda não possui inibidores para serem direcionados às etapas clínicas do desenvolvimento de novos fármacos, tornando-se relevante a identificação e caracterização de novas moléculas que possam atuar como inibidores seletivos desta proteína. Neste contexto, 13 derivados de magnolol vem sendo testados quanto à capacidade de inibir o transportador ABCG2.Dois compostos, CT_M10 e CT_M15, apresentaram capacidade inibitória frente ao transportador com valores de IC_{50} de 22,6 e 9,5 µM, respectivamente. Ambos os compostos foram seletivos para ABCG2 quando testados frente a transportador P-gp. Além disso, ambos os compostos apresentaram citotoxicidade consideravelmente baixa, destacando-se o CT_M15 com valor de IG_{50} de citotoxicidade superior a 100 µM e razão terapêutica (RT) (citotoxicidade / inibição), superior a 10. Foi demonstrado que a ligação do CT_M15 ao transportador ABCG2 apresenta efeitos sobre a atividade ATPase e termoestabilidade da proteína, desestabilizando sua estrutura. O composto também foi capaz de inibir o efluxo de diferentes substratos. Ademais, CT_M15 não demonstrou impactos nos níveis de expressão de mRNA de ABCG2, promoveu aumento no reconhecimento do anticorpo conformacional 5D3 e apresentou inibição do tipo mista. Por fim foram identificados, através de docking molecular, diferentes sítios de ligação entre o substrato mitoxantrona e CT_M15. Estes dados demonstram que o CT_M15 é um promissor inibidor seletivo de ABCG2, apresentando mínima citotoxicidade, uma característica importante a ser buscada em futuros ensaios pré-clínicos. Ainda buscando alternativas para combater a resistência à quimioterapia, o presente estudo descreveu um equipamento a base de LED, simples e de baixo custo para realização de terapia fotodinâmica com todos os detalhes de construção e programação. Como prova de conceito, o equipamento foi utilizado para promover um aumento na sensibilização de células HeLa tratadas com o fotossensibilizador verteporfin. Os resultados foram comparados com um equipamento comercial a base de LED (LumaCare®) e os efeitos citotóxicos observados foram associados à geração de espécies reativas de oxigênio (ROS), demonstrando que o equipamento representa uma promissora alternativa para estudos *in vitro* de PDT.

Palavras-chave: resistência à múltiplas drogas (MDR); ABCG2; inibidores; magnolol; terapia fotodinâmica (PDT).

ABSTRACT

Cancer is one of the diseases with the highest mortality rate in the world and the emergence of resistance to the conventional chemotherapy exacerbates this problem. Several mechanisms related to multidrug resistance (MDR) in cancer have been described, however the overexpression of ABC transporters is considered the main cause of this clinical condition. The human genome encodes 48 ABC transporters, among which 3 are highlighted for their involvement in the MDR phenotype: P-glycoprotein (P-gp or MDR1), multidrug resistance associated protein-1 (MRP1) and breast cancer resistance protein (BCRP or ABCG2). These three transporters can recognize a broad spectrum of chemically unrelated antineoplastic agents and promote their efflux; therefore, new compounds have been studied to inhibit the transport mediated by these proteins. Although ABCG2 is one of the three ABC transporters with the highest involvement in MDR, there are still no inhibitors to be forwarded to clinical steps of drug development, which makes the identification and characterization of new selective inhibitors of this protein very important. In this context, 13 magnolol derivatives have been tested for their ability to inhibit the ABCG2 transporter. Two compounds, CT_M10 and CT_M15, were capable to inhibit the transport activity, showing IC_{50} values of 22.6 and 9.5 µM, respectively. Both compounds were selective toward ABCG2 when tested against P-gp. In addition, both inhibitors showed a very low-cytotoxic effect, especially CT_M15 which showed an IG_{50} value of cytotoxicity higher than 100 µM and a therapeutic ratio (TR) (cytotoxicity/inhibition) higher than 10. CT_M15 binding has been shown to affect the ATPase activity and thermostability of ABCG2, destabilizing the protein structure. This compound was capable to inhibit the efflux of different substrates. In addition, CT_M15 showed no effects on mRNA expression levels of ABCG2, promoted an increase on the recognition of 5D3 conformational antibody and performed a mixed type of inhibition. Finally, it was identified by molecular docking different binding sites between the substrate mitoxantrone and CT_M15. These data demonstrate that CT_M15 is a promising selective inhibitor of ABCG2 showing minimal cytotoxicity, an important feature to pursue in future preclinical trials. Still looking for alternatives to combat resistance to chemotherapy, the present study described a simple and low-cost LED-based device for performing photodynamic therapy (PDT) with all construction and programming details. As a proof of concept, the equipment was used to promote an increase in the sensitization of HeLa cells treated with the photosensitizer verteporfin. The results were compared with a commercial LED-based device (LumaCare®) and the observed cytotoxic effects were associated with the generation of reactive oxygen species (ROS), demonstrating that the device represents a promising alternative for *in vitro* studies of PDT.

Keywords: multidrug resistance (MDR); ABCG2; inhibitors; magnolol; photodynamic therapy (PDT).

FIGURE LIST

TABLE LIST

LIST OF ABBREVIATIONS

ABC	ATP binding cassette
ABCP	ATP binding cassette placenta
ATP	Adenosine Triphosphate
BCRP	Breast Cancer Resistance Protein
BLAST	Basic Local Alignment Search Tool
BLAT	BLAST-like Alignment Tool
BSA	Bovine serum albumine
CAPES	Coordenação de aperfeiçoamento de pessoal de nível superior
CCT	Correlated color temperature
CNC	Computadorized numerical control
CNPq	Conselho nacional de desenvolvimento científico e tecnológico
Cryo-EM	Cryogenic electron mycroscopy
DCF	2',7'-dichlorofluorescein
DCFDA	2',7'-dichlorohydrofluorescein diacetate
DMEM	Dulbecco's Modified Eagle's Medium
DMSO	Dimethyl sulfoxide
DTT	Dithiothreitol
EDTA	Etheylenediaminetetraacetic acid
EGTA	Ethylene-bis(oxyethylenenitrilo)tetraacetic acid
FACS	Fluorescence-activated single cell sorting
FBS	Fetal bovine serum
FDA	Food & Drug Administration
FTC	Fumitremorgin C
IC_{50}	Concentration that inhibits 50% of maximum inhibition
IDE	Integrated development environment
IG_{50}	Concentration that 50% of population survive
IT_{50}	Temperature that reduces 50% of the ATPase activity
K_m	Michaelis Menten constant
LCD	Liquid crystal display
LED	Light-emitting-diode
MBE	Magnolia bark extracts
MDF	Medium-density fiberboard
MDR	Multidrug Resistance
MRP1	Multidrug Resistance Protein 1
MTT	3-(4,5-dimethylthiazol-2-yl)-2,5-iphenyltetrazolium bromide
MTX	Mitoxantrone
MXR	Mitoxantrone Resistance
NCBI	National Center for Biotechonology Information
NMDG	N-methyl-D-glucamine
PBS	Phosphate Buffer Solution
PDB	Protein Data Bank
PDT	Photdynamic Therapy

P-gp	P-glycoprotein
PPSUS	Programa Pesquisa para o SUS
PS	Photosensitizer
qPCR	Quantitative polymerase chain reaction
RGB	Red green blue
ROS	Reactive oxygen species
SAR	Structure-activity relationship
SDS	Sodium Dodecyl Sulfate
SPI	Serial peripheral interface
SUS	Sistema Único de Saúde
TR	Therapeutic Ratio
USB	Universal serial bus
V_{max}	Maximum efflux at saturation
WT	Wild-type

SUMMARY

THESIS OVERVIEW

The findings described on this thesis bring new insights about ABCG2 inhibitors derived from natural scaffolds and the development of an open-source equipment for photodynamic therapy (PDT). This document was conceived as described below:

- An introduction about the general aspects of multidrug resistance related to cancer, including two strategies for overcome MDR that guided the execution of this work.
- Chapter 1 shows the identification and characterization of the magnolol derivative named here as **CT_M15**, as a new selective and noncytotoxic ABCG2 inhibitor.
- Chapter 2 describes the in-house development of a simple and low-cost LED-based photodynamic therapy device designed for *in vitro* assays.

1 INTRODUCTION

Among the most lethal noncommunicable diseases, cancer represents the main cause of premature death and, consequently, an important barrier to the increase in global life expectancy. According to estimates by the World Health Organization the disease was responsible for approximately one in six deaths worldwide, accounting for about 10 million deaths only in 2020 [1].

Chemotherapy protocols remain the leading therapeutic approach for the treatment of neoplastic diseases [2], nonetheless, they present two serious aggravating factors: costs and ineffectiveness rates. In Brazil, oncology services consumed from public coffers in 2016 the colossal amount of R$ 12.481.315,04, exclusively related to medicines offered by the national unified health system, SUS BRASIL, M. DA S. (2016). Additionally, post-chemotherapy survival rates are discouraging, and this failure is mostly due to the phenomenon of multidrug resistance (MDR) related to cancer [4].

Neoplastic cells can develop resistance to chemotherapy through several biological mechanisms, such as reduced uptake of drugs, activation of detoxifying systems, alterations in drug metabolism, apoptosis failure, changes of molecular drug targets among others [5–8], but the increase in the efflux of substances mediated by transmembrane proteins called ABC transporters stands out as the main cause of MDR within the tumor microenvironment [9]. Exporters of a wide variety of substrates in eukaryotic cells [10], these proteins play an important physiological role in detoxification processes and maintenance of body homeostasis in healthy organisms [11–13]; conversely, when overexpressed in the plasma membrane of cancer cells, ABC transporters involved in MDR process prevent the intracellular accumulation of antineoplastic agents avoiding the drug-induced cell death [14,15].

The human genome encodes 48 ABC proteins organized in seven subfamilies (ABCA-ABCG) [16,17], among which 3 stand out in terms of their close involvement with the MDR phenotype: glycoprotein-P (P-gp/*ABCB1* or MDR1), multidrug resistance protein 1 (MRP1/*ABCC1*) and breast cancer resistance protein (BCRP/*ABCG2* or ABCG2 protein) [18,19]. The first identified ABC transporter related to MDR was P-gp, discovered in 1976 and firstly described in a Chinese ovary tissue culture cells resistant

to colchicine with cross-resistance to other chemotherapeutics [20,21]. MRP1 was the second member of the superfamily of ABC transporters to be identified and related to MDR, in 1992 by Cole et al., who reported the existence of a second drug efflux pump, similar to the already known P-gp, in a human cell line (NCI-H69 – small-cell lung carcinoma) by doxorubicin selection [22]. The most recently discovered ABC transporter was identified simultaneously by three different laboratories in 1998: (i) Doyle et al. described the protein overexpression utilizing breast cancer cell line (MCF-7 resistant to adriamycin and verapamil) and named the transporter as Breast Cancer Resistance Protein (BCRP) [23]; (ii) Miyake et al. verified ABCG2 overexpression on human colon carcinoma cell line (S1-M1-80 resistant to mitoxantrone) and adopted the nomenclature Mitoxantrone Resistance (MXR) [24]; (iii) Allikmets et al. stated the same phenomenon with human placenta tissue, which led them to name the protein as ATP-Binding Cassette Placenta (ABCP) [25].

The use of inhibitors of the efflux activity exerted by ABC transporters in association with chemotherapy protocols is considered the most promising strategy to reverse MDR and, for this reason, the last few years have been marked by the massive investment of scientific efforts for protein structural elucidation and identification of selective inhibitors of these proteins [26–35].

Some characteristics must be considered during the process of identification, design and development of new inhibitors and are crucial for obtaining safe and effective compounds: (i) having high affinity for the target transporter, resulting in efficacy at low concentrations, (ii) being specific for just one transporter, since the simultaneous inhibition of multiple ABC transporters can negatively impact the natural process of cellular detoxification and homeostasis of a healthy organism (iii) to not perform pharmacokinetic interactions with co-administered chemotherapeutic drugs, (iv) to not be transported (recognized as a substrate) by the target protein, and, consequently, remain bound to the transporter long enough for performing successful inhibition and (v) exhibit low cytotoxicity [36].

To date, only P-gp inhibitors have been submitted to clinical tests, however, their use has not yet been included in the clinical routine as a consequence of mostly unsatisfactory results emphasizing the need to inhibit other ABC transporters, essentially ABCG2 [14,30,37,38]. Thus, the identification of specific inhibitors of the ABCG2 transporter with satisfactory levels of safety and efficacy so that they can be taken to clinical trials is urgent.

It is important to emphasize that ABCG2 has a wide substrate specificity, with a relative preference for hydrophobic, flat and polycyclic compounds [39] and, as a consequence, a considerable variety of chemotherapeutic agents constitute the list of ABCG2 substrates, such as methotrexate, mitoxantrone, inhibitors of topoisomerases I or II, such as topotecan and doxorubicin, and SN-38 (irinotecan's active metabolite). This fact contributes to explain several failures observed in the current therapeutic regimen applied to cancer [40].

As it is the most recently discovered ABC transporter directly related to MDR, the process of development of ABCG2 inhibitors is not at such advanced stages as glycoprotein-P, but its potential as an adjuvant in pharmacological regimens, especially chemotherapy protocols, garnered major efforts to identify specific protein inhibitors [14].

The first ABCG2 inhibitor identified was the fungal toxin fumitremorgin C (FTC), that is selective for ABCG2, however it showed undesirable neurotoxic effects, and, for this reason, it had its development discontinued. To reduce neurotoxicity, tetracyclic analogues of FTC were developed, among which Ko143 deserves to be highlighted for having greater potency and lower toxic rates than its precursor. Despite the highlighted improvements, Ko143 was not stable in mouse plasma and presented non-specific effects when in high concentrations, also inhibiting P-gp and MRP1. Efforts were also invested in the development of selective ABCG2 inhibitors that are derived from tariquidar, a third generation P-gp inhibitor [35].

The last few years have been marked by efforts aimed to identify selective and non-toxic ABCG2 inhibitors through the structural modification of already known inhibitors. These are series of chemically unrelated compounds - such as flavones [41], chromones [42], chalcones [43], indeno[1,2-b]indoles [44], porphyrins [45] and others (Fig. 1). Still, following the major focus of the new inhibitors development process (chemical changes in the molecular scaffold of already identified inhibitors), groups have been focusing on the identification of new ABCG2 inhibitors through virtual screening based on ligands of compounds contained in the drug database approved by the U.S. FDA [46].
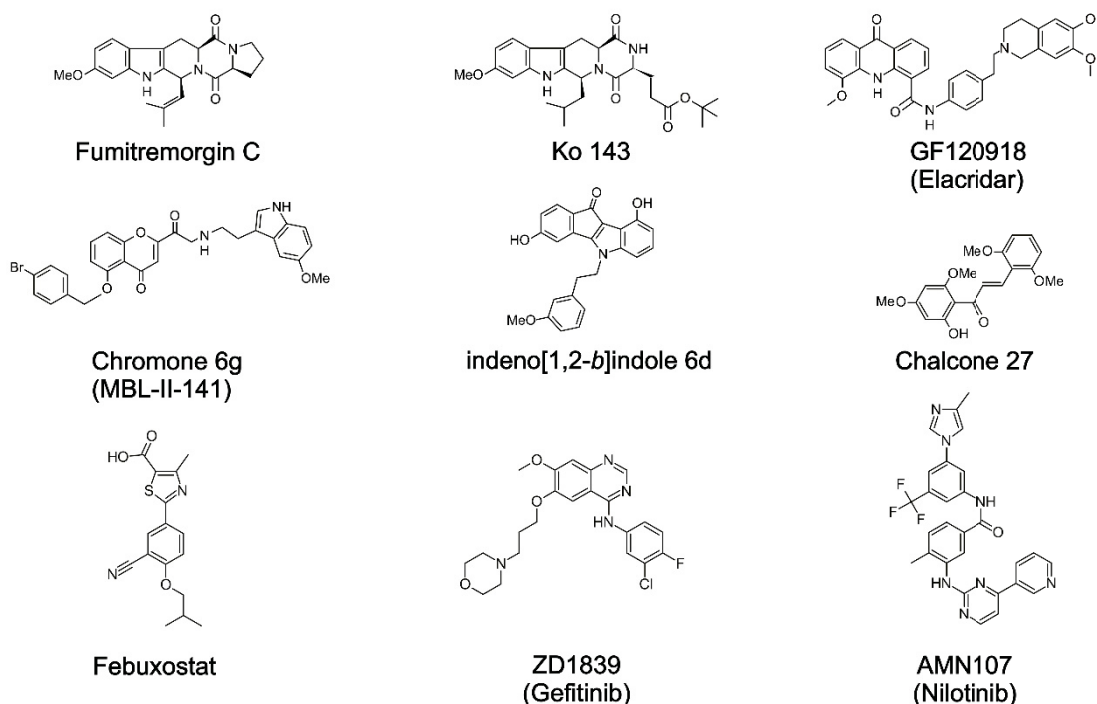
Figure 1 – Chemical structure of ABCG2 inhibitors. All these compounds were described as ABCG2 inhibitors.

Natural products are a great source of chemical scaffolds for new drugs and represent a powerful source for ABCG2 inhibitors [47]. Flavonoids [48], botryllamides [49], polyphenols [50] are among the natural compounds identified as inhibitors of ABCG2 that were latter modified to improve their activity. It is interesting to notice that those classes share some characteristics as hydrophobicity, aromaticity, and planar structure.

The scientific community have been demonstrating an increasing interest in the beneficial properties of plant polyphenols. In addition to being widely exploited in the pharmaceutical, cosmetic, and food industries [51], several phenolic compounds, naturally found in foods that constitute the daily diet of the majority of the population, stand out as important preventive agents against degenerative diseases [52].

Among the most widely researched polyphenols, two compounds have shown numerous and increasing research data in recent years: magnolol and its isomer honokiol, which have a biphenolic nucleus with two allylic side chains (Fig. 2). These are dimeric neolignanes, therefore, and represent the main biologically active components of *Magnolia spp*. (MBE – Magnolia bark extracts) [53]. Naturally,

magnolol/honokiol contents in extracts directly depends on plant aspects – such as species, geographic origin and part of the plant used – and formulation methods [54].
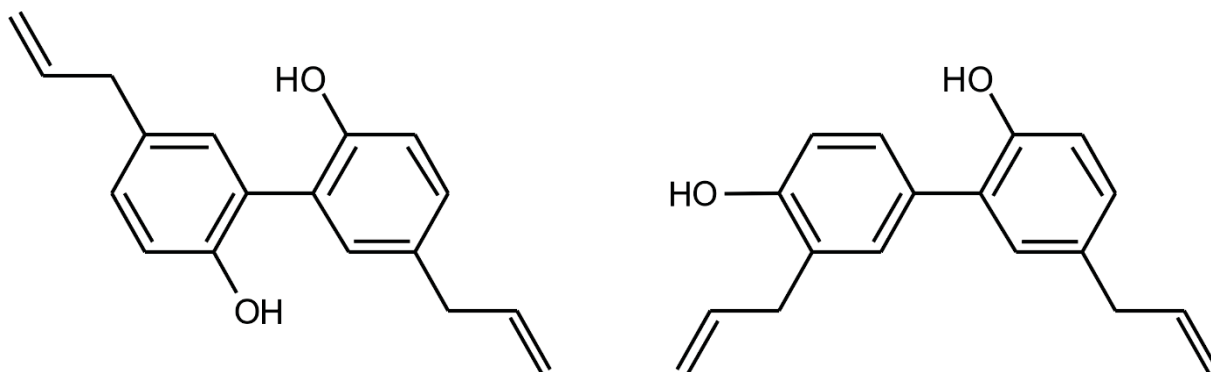
Figure 2 – Chemical structure of both isomers of magnolol. Magnolol (left) and honokiol (right).

Magnolia officinalis and *Magnolia obovata* emerge among the numerous species of magnolia and are widely used in the ancient practice of traditional Chinese, Japanese and Korean medicines. The wide range of medicinal properties of these two species corroborates their extended use to modern clinical practices [54]. Historically, parts of the tree's root and stem were widely used to combat gastrointestinal disorders, anxiety, allergies, and acute pain. Subsequently, important biological activities were also related to the plant, such as muscle relaxation in addition to antioxidant, antimicrobial, anti-inflammatory and sedative effects [52,55].

Magnolol can cross the blood brain barrier with ease [55] and its oral bioavailability is approximately 10%. The compound presents tissue (mainly hepatic) and enzymatic (intestinal microbiome) metabolization, with a variety of subproducts, such as hydrogenated and hydroxylated derivatives, sulfates, and glucuronides. Accordingly, the glucuronidation process is common to the metabolism of many other dietary polyphenols [56–59]. The substance also has a rapid pattern of renal clearance and short and long-term preclinical studies have not identified physiological alterations resulting from the administration of magnolol-based preparations [54,59,60].

Numerous preclinical studies have verified an antitumoral activity exerted by magnolol against different types of cancer, such as lung, prostate, breast, gallbladder, colon, skin and liver [61–67]. The molecular mechanisms that confer antitumor activity to magnolol correspond to the reduction of cell proliferation, induction of apoptosis,

increased generation of reactive oxygen species (ROS), induction of autophagy and activation/inactivation of cell signaling [52].

In vitro and, subsequently, in vivo studies have shown that magnolol has a satisfactory safety profile [68,69], contributes to the reduction of tumor growth, induces apoptosis and inhibits invasion, migration and metastasis [52,67,70]. Additionally, studies suggest that magnolol, honokiol and 4-O-methylhonokiol may be promising agents in combating MDR through negative regulation of P-gp (ABCB1) expression [71]. More recently, the two isomers were described as promising inhibitors of ABCG2 function and expression [60].

Researchers have been focusing on the determination of synthetic routes - with good cost and yield ratios - to obtain magnolol derivatives as well as their respective biological characteristics. Some compounds, synthetically obtained from chemical replacements and/or insertions carried out in the main structural core of magnolol, showed inhibitory activities against tankyrase-2 [72] and yeasts α-glucosidase enzymes. The latter is also a promising property when considering the optimized development of new antidiabetic drugs [73].

As for the structure-activity relationship (SAR), infrared spectroscopy and theoretical calculations were conducted to verify alterations or preservation of characteristics observed in the synthesized derivatives compared to the precursor molecule. The introduction of hydroxyl groups ortho to the phenolic OH in magnolol structure represents a good strategy for obtaining derivatives with increased antioxidant properties. The opposite was observed in the di-methoxylated derivatives of magnolol, and no effect was described in derivatives obtained from the insertion of both groups, hydroxy and methoxy, in the original structure [74]. Magnolol derivatives were identified and characterized as potent and selective ABCG2 inhibitors, and more details can be accessed on chapter 1 of this work.

Considering the challenging scenario presented by MDR related to chemotherapy, some other therapeutic approaches have been studied and photodynamic therapy (PDT) represents a feasible option for both single and adjuvant cancer treatment [75–77]. The antitumor effect is obtained through selective ROS-mediated cell death as a result of a combination of chemical (photosensitizer compounds) and physical (light irradiation) treatment. PDT is also superior to conventional methods, including chemotherapy, in terms of costs and undesirable side-effects [78,79].

Several studies have been conducted in the past decades since the first report describing positive results obtained through the technique was published in 1975 [75,80]. *In vitro* and *in vivo* models employing photosensitizers associated to irradiation reported positive outcomes, which encourages regulatory agencies to evaluate the clinical use of this category of compounds [81–85].

The classical light source for PDT consists of diode laser systems, which present a range of drawbacks related to costs and complexity of utilization and maintenance [86–88]. Differently, light-emitting-diode (LED) equipment represent an advantageous solution not only for costs and complexity but also for performance efficiency, which converts this category of machinery to the preference of several research groups [89–91].

Commercial LED-based PDT devices are still economically unaffordable for most research groups around the globe and this fact has encouraged multidisciplinary groups to develop prototypes to meet this demand and allow PDT research to continue taking place in the antitumoral approaches area [87,92–96]. With the aim of contributing to this long journey of development and validation of economical LED-based PDT equipment, an open source, low cost and in-house-built prototype is presented in chapter 2 of this work.

2 REFERENCES

[1]   WHO, Assesing National Capacity For The Prevention and Control of Noncommunicable Diseases : Report of the 2019 Global Survey, 2020. https://www.who.int/publications/i/item/ncd-ccs-2019.

[2]   L. Falzone, S. Salomone, M. Libra, Evolution of cancer pharmacological treatments at the turn of the third millennium, Front. Pharmacol. 9 (2018). https://doi.org/10.3389/fphar.2018.01300.

[3]   B. Fleisher, J. Unum, J. Shao, G. An, Ingredients in fruit juices interact with dasatinib through inhibition of BCRP: a new mechanism of beverage-drug interaction., J. Pharm. Sci. 104 (2015) 266–275. https://doi.org/10.1002/jps.24289.

[4]   Z. Chen, T. Shi, L. Zhang, P. Zhu, M. Deng, C. Huang, T. Hu, L. Jiang, J. Li, Mammalian drug efflux transporters of the ATP binding cassette (ABC) family in multidrug resistance: A review of the past decade., Cancer Lett. 370 (2016) 153–164. https://doi.org/10.1016/j.canlet.2015.10.010.

[5]   Y.A. Luqmani, Mechanisms of drug resistance in cancer chemotherapy, Med. Princ. Pract. 14 (2005) 35–48. https://doi.org/10.1159/000086183.

[6]   K. Bukowski, M. Kciuk, R. Kontek, Mechanisms of multidrug resistance in cancer chemotherapy, Int. J. Mol. Sci. 21 (2020). https://doi.org/10.3390/ijms21093233.

[7]   Q. Wu, Z. Yang, Y. Nie, Y. Shi, D. Fan, Multi-drug resistance in cancer chemotherapeutics: Mechanisms and lab approaches, Cancer Lett. 347 (2014) 159–166. https://doi.org/10.1016/j.canlet.2014.03.013.

[8]   S.M. Simon, M. Schindler, Cell biological mechanisms of multidrug resistance in tumors, Proc. Natl. Acad. Sci. U. S. A. 91 (1994) 3497–3504. https://doi.org/10.1073/pnas.91.9.3497.

[9]   G. Szakacs, J.K. Paterson, J.A. Ludwig, C. Booth-Genthe, M.M. Gottesman, G. Szakács, J.K. Paterson, J.A. Ludwig, C. Booth-Genthe, M.M. Gottesman, Targeting multidrug resistance in cancer, Nat. Rev. Drug Discov. 5 (2006) 219–234. https://doi.org/10.1038/nrd1984.

[10]   C.F. HIGGINS, Abc Transporters - From Microorganisms To Man, Annu. Rev. Cell Biol. 8 (1992) 67–113.

[11]   I.S. Mohammad, W. He, L. Yin, Understanding of human ATP binding cassette superfamily and novel multidrug resistance modulators to overcome MDR, Biomed. Pharmacother. 100 (2018) 335–348. https://doi.org/10.1016/j.biopha.2018.02.038.

[12]   K.J. Linton, Structure and function of ABC transporters, Physiology. 22 (2007) 122–130. https://doi.org/10.1152/physiol.00046.2006.

[13]   I.B. Holland, ABC transporters, mechanisms and biology: An overview, Essays Biochem. 50 (2011) 1–17. https://doi.org/10.1042/BSE0500001.

[14]   R.W. Robey, K.M. Pluchino, M.D. Hall, A.T. Fojo, S.E. Bates, M.M. Gottesman, Revisiting the role of ABC transporters in multidrug-resistant cancer, Nat. Rev. Cancer. 18 (2018) 452–464. https://doi.org/10.1038/s41568-018-0005-8.

[15]   R.W. Robey, S. Shukla, E.M. Finley, R.K. Oldham, D. Barnett, S. V. Ambudkar, T. Fojo, S.E. Bates, Inhibition of P-glycoprotein (ABCB1)- and multidrug resistance-associated protein 1 (ABCC1)-mediated transport by the orally administered inhibitor, CBT-1®, Biochem. Pharmacol. 75 (2008) 1302–1312. https://doi.org/10.1016/j.bcp.2007.12.001.

[16]   M. Dean, The genetics of ATP-binding cassette transporters, Methods Enzymol. 400 (2005) 409–429. https://doi.org/10.1016/S0076-6879(05)00024-8.

[17]   R. Allikmets, M. Dean, A. Rzhetsky, The Human ATP-Binding Cassette (ABC) Transporter Superfamily, Cancer Res. 4 (2001) 1156–1166. https://doi.org/10.1101/gr.184901.The.

[18]   G. Szakács, A. Váradi, C. Özvegy-Laczka, B. Sarkadi, The role of ABC transporters in drug absorption, distribution, metabolism, excretion and toxicity (ADME-Tox), Drug Discov. Today. 13 (2008) 379–393. https://doi.org/10.1016/j.drudis.2007.12.010.

[19]   Y.H. Choi, A.-M. Yu, ABC transporters in multidrug resistance and pharmacokinetics, and strategies for drug development., Curr. Pharm. Des. 20 (2014) 793–807.

[20]   R.L. Juliano, V. Ling, A surface glycoprotein modulating drug permeability in Chinese hamster ovary cell mutants, BBA - Biomembr. 455 (1976) 152–162. https://doi.org/10.1016/0005-2736(76)90160-7.

[21]   A.H. Schinkel, J.J.M. Smit, O. van Tellingen, J.H. Beijnen, E. Wagenaar, L. van Deemter, C.A.A.M. Mol, M.A. van der Valk, E.C. Robanus-Maandag, H.P.J. te Riele, A.J.M. Berns, P. Borst, Disruption of the mouse mdr1a P-glycoprotein gene leads to a deficiency in the blood-brain barrier and to

increased sensitivity to drugs, Cell. 77 (1994) 491–502. https://doi.org/10.1016/0092-8674(94)90212-7.

[22] S.P.C. Cole, G. Bhardwaj, J.H. Gerlach, J.E. Mackie, C.E. Grant, K.C. Almquist, A.J. Stewart, E.U. Kurz, A.M.V. Duncan, R.G. Deeley, Overexpression of a transporter gene in a multidrug-resistant human lung cancer cell line, Science (80-.). 258 (1992) 1650–1654. https://doi.org/10.1126/science.1360704.

[23] L.A. Doyle, W. Yang, L. V Abruzzo, T. Krogmann, Y. Gao, A.K. Rishi, D.D. Ross, A multidrug resistance transporter from human MCF-7 breast cancer cells., Proc. Natl. Acad. Sci. U. S. A. 95 (1998) 15665–15670.

[24] K. Miyake, L. Mickley, T. Litman, Z. Zhan, R. Robey, B. Cristensen, M. Brangi, L. Greenberger, M. Dean, T. Fojo, S.E. Bates, Molecular Cloning of cDNAs Which Are Highly Overexpressed in Mitoxantrone-resistant Cells, Cancer Res. 59 (1999) 8–13.

[25] R. Allikmets, L.M. Schriml, A. Hutchinson, V. Romano-Spica, M. Dean, A human placenta-specific ATP-binding cassette gene (ABCP) on chromosome 4q22 that is involved in multidrug resistance, Cancer Res. 58 (1998) 5337–5339.

[26] A. Tamaki, C. Ierano, G. Szakacs, R.W. Robey, S.E. Bates, The controversial role of ABC transporters in clinical oncology., Essays Biochem. 50 (2011) 209–232. https://doi.org/10.1042/bse0500209.

[27] S.L. Allen, E. Velez-garcia, J.O. Moore, T.C. Shea, E. Hoke, Dose Escalation Studies of Cytarabine , Daunorubicin , and Etoposide With and Without Multidrug Resistance Modulation With PSC-833 in Untreated Adults With Acute Myeloid Leukemia Younger Than 60 Years : Final Induction Resu, J. Clin. Oncol. 22 (2015). https://doi.org/10.1200/JCO.2004.11.106.

[28] W.R. Friedenberg, M. Rue, E.A. Blood, W.S. Dalton, C. Shustik, R.A. Larson, P. Sonneveld, P.R. Greipp, Phase III study of PSC-833 (valspodar) in combination with vincristine, doxorubicin, and dexamethasone (valspodar/VAD) versus VAD alone in patients with recurring or refractory multiple myeloma (E1A95): A trial of the Eastern Cooperative Oncology Group, Cancer. 106 (2006) 830–838. https://doi.org/10.1002/cncr.21666.

[29] J. Abraham, M. Edgerly, R. Wilson, C. Chen, A. Rutt, S. Bakke, R. Robey, A. Dwyer, B. Goldspiel, F. Balis, O. Van Tellingen, S.E. Bates, T. Fojo, Clinical A Phase I Study of the P-Glycoprotein Antagonist Tariquidar in Combination with Vinorelbine, Cancer Ther. 15 (2009) 3574–3583. https://doi.org/10.1158/1078-0432.CCR-08-0938.

[30] E. Fox, S.E. Bates, Tariquidar (XR9576): A P-glycoprotein drug efflux pump inhibitor, Expert Rev. Anticancer Ther. 7 (2007) 447–459. https://doi.org/10.1586/14737140.7.4.447.

[31] C. Lhommé, F. Joly, J.L. Walker, A.A. Lissoni, M.O. Nicoletto, G.M. Manikhas, M.M.O. Baekelandt, A.N. Gordon, P.M. Fracasso, W.L. Mietlowski, G.J. Jones, M.H. Dugan, Phase III study of valspodar (PSC 833) combined with paclitaxel and carboplatin compared with paclitaxel and carboplatin alone in patients with stage IV or suboptimally debulked stage III epithelial ovarian cancer or primary peritoneal cancer, J. Clin. Oncol. 26 (2008) 2674–2682. https://doi.org/10.1200/JCO.2007.14.9807.

[32] H. Wang, X. Li, T. Chen, W. Wang, Q. Liu, H. Li, J. Yi, J. Wang, Mechanisms of verapamil-enhanced chemosensitivity of gallbladder cancer cells to

platinum drugs: Glutathione reduction and MRP1 downregulation, Oncol. Rep. 29 (2013) 676–684. https://doi.org/10.3892/or.2012.2156.

[33] S.M. Stefan, M. Wiese, Small-molecule inhibitors of multidrug resistance-associated protein 1 and related processes: A historic approach and recent advances, Med. Res. Rev. 39 (2019) 176–264. https://doi.org/10.1002/med.21510.

[34] F. Marighetti, K. Steggemann, M. Karbaum, M. Wiese, Scaffold identification of a new class of potent and selective BCRP inhibitors., ChemMedChem. 10 (2015) 742–751. https://doi.org/10.1002/cmdc.201402498.

[35] S.M. Jackson, I. Manolaridis, J. Kowal, M. Zechner, N.M.I. Taylor, M. Bause, S. Bauer, R. Bartholomaeus, G. Bernhardt, B. Koenig, A. Buschauer, H. Stahlberg, K. Altmann, K.P. Locher, Structural basis of small-molecule inhibition of human multidrug transporter ABCG2, Nat. Struct. Mol. Biol. 25 (2018). https://doi.org/10.1038/s41594-018-0049-1.

[36] A. Boumendjel, S. Macalou, G. Valdameri, A. Pozza, C. Gauthier, O. Arnaud, E. Nicolle, S. Magnard, P. Falson, R. Terreux, P.-A. Carrupt, L. Payen, A. Di Pietro, Targeting the Multidrug ABCG2 Transporter with Flavonoidic Inhibitors: In Vitro Optimization and In Vivo Validation., Curr Med Chem. 18 (2011) 3387–3401. https://doi.org/10.2174/092986711796504736.

[37] F.S. Chung, J.S. Santiago, M.F.M. De Jesus, C. V. Trinidad, M.F.E. See, Disrupting P-glycoprotein function in clinical settings: What can we learn from the fundamental aspects of this transporter?, Am. J. Cancer Res. 6 (2016) 1583–1598.

[38] F. Morschhauser, P.L. Zinzani, M. Burgess, L. Sloots, F. Bouafia, C. Dumontet, Phase I/II trial of a P-glycoprotein inhibitor, Zosuquidar.3HCl trihydrochloride (LY335979), given orally in combination with the CHOP regimen in patients with non-Hodgkin's lymphoma, Leuk. Lymphoma. 48 (2007) 708–715. https://doi.org/10.1080/10428190701190169.

[39] I. Manolaridis, S.M. Jackson, N.M.I. Taylor, J. Kowal, H. Stahlberg, K.P. Locher, Cryo-EM structures of a human ABCG2 mutant trapped in ATP-bound and substrate-bound states, Nature. 563 (2018) 426–430. https://doi.org/10.1038/s41586-018-0680-3.

[40] D. Peña-Solorzano, S.A. Stark, B. König, C.A. Sierra, C. Ochoa-Puentes, ABCG2/BCRP: Specific and Nonspecific Modulators, Med. Res. Rev. 37 (2017) 987–1050. https://doi.org/10.1002/med.

[41] J. Gallus, K. Juvale, M. Wiese, Characterization of 3-methoxy flavones for their interaction with ABCG2 as suggested by ATPase activity., Biochim. Biophys. Acta. 1838 (2014) 2929–2938. https://doi.org/10.1016/j.bbamem.2014.08.003.

[42] G. Valdameri, E. Genoux, B. Peres, Substituted chromones as highly potent nontoxic inhibitors, specific for the breast cancer resistance protein., J. Med. Chem. 55 (2012) 3193–3200. https://doi.org/10.1021/jm2016528.Investigation.

[43] G. Valdameri, C. Gauthier, R. Terreux, R. Kachadourian, B.J. Day, S.M.B. Winnischofer, M.E.M. Rocha, V. Frachet, X. Ronot, A. Di Pietro, A. Boumendjel, Investigation of chalcones as selective inhibitors of the breast cancer resistance protein: Critical role of methoxylation in both inhibition potency and cytotoxicity, J. Med. Chem. 55 (2012) 3193–3200. https://doi.org/10.1021/jm2016528.

[44]   D.H. Kita, N. Guragossian, I.F. Zattoni, V.R. Moure, F.G. de M. Rego, S. Lusvarghi, T. Moulenat, B. Belhani, G. Picheth, S. Bouacida, Z. Bouaziz, C. Marminon, M. Berredjem, J. Jose, M.B. Gonçalves, S. V. Ambudkar, G. Valdameri, M. Le Borgne, Mechanistic basis of breast cancer resistance protein inhibition by new indeno[1,2-b]indoles, Sci. Rep. 11 (2021) 1–16. https://doi.org/10.1038/s41598-020-79892-w.

[45]   I.F. Zattoni, T. Kronenberger, D.H. Kita, L.D. Guanaes, M.M. Guimarães, L. de Oliveira Prado, M. Ziasch, L.C. Vesga, F. Gomes de Moraes Rego, G. Picheth, M.B. Gonçalves, M.D. Noseda, D.R.B. Ducatti, A. Poso, R.W. Robey, S. V. Ambudkar, V.R. Moure, A.G. Gonçalves, G. Valdameri, A new porphyrin as selective substrate-based inhibitor of breast cancer resistance protein (BCRP/ABCG2), Chem. Biol. Interact. 351 (2022). https://doi.org/10.1016/j.cbi.2021.109718.

[46]   Y. Pan, P.P. Chothe, P.W. Swaan, Identification of novel breast cancer resistance protein (BCRP) inhibitors by virtual screening., Mol. Pharm. 10 (2013) 1236–1248. https://doi.org/10.1021/mp300547h.

[47]   A. Kumar, V. Jaitak, Natural products as multidrug resistance modulators in cancer, Eur. J. Med. Chem. 176 (2019) 268–291. https://doi.org/10.1016/j.ejmech.2019.05.027.

[48]   S. Zhang, X. Yang, M.E. Morris, Flavonoids are inhibitors of breast cancer resistance protein (ABCG2)-mediated transport., Mol. Pharmacol. 65 (2004) 1208–1216. https://doi.org/10.1124/mol.65.5.1208.

[49]   C.J. Henrich, R.W. Robey, K. Takada, H.R. Bokesch, S.E. Bates, S. Shukla, S. V Ambudkar, J.B. Mcmahon, K.R. Gustafson, Botryllamides: Natural Product Inhibitors of ABCG2, ACS Chem. Biol. 4 (2009) 637–647.

[50]   S. Shukla, H. Zaher, A. Hartz, B. Bauer, J.A. Ware, S. V. Ambudkar, Curcumin inhibits the activity of ABCG2/BCRP1, a multidrug resistance-linked ABC drug transporter in mice, Pharm. Res. 26 (2009) 480–487. https://doi.org/10.1007/s11095-008-9735-8.

[51]   R. Ciriminna, F. Meneguzzo, R. Delisi, M. Pagliaro, Citric acid: Emerging applications of key biotechnology industrial product, Chem. Cent. J. 11 (2017) 1–9. https://doi.org/10.1186/s13065-017-0251-y.

[52]   Y.J. Lee, Y.M. Lee, C.K. Lee, J.K. Jung, S.B. Han, J.T. Hong, Therapeutic applications of compounds in the Magnolia family, Pharmacol. Ther. 130 (2011) 157–176. https://doi.org/10.1016/j.pharmthera.2011.01.010.

[53]   Y.J. Surh, Cancer chemoprevention with dietary phytochemicals, Nat. Rev. Cancer. 3 (2003) 768–780. https://doi.org/10.1038/nrc1189.

[54]   A. Sarrica, N. Kirika, M. Romeo, M. Salmona, L. Diomede, Safety and Toxicology of Magnolol and Honokiol, Planta Med. (2018). https://doi.org/10.1055/a-0642-1966.

[55]   T.H. Tsai, C.J. Chou, C.F. Chen, Disposition of magnolol after intravenous bolus and infusion in rabbits, Drug Metab. Dispos. 22 (1994) 518–521. https://doi.org/10.1111/j.2042-7158.1996.tb05877.x.

[56]   K. Yang, N.D. Pfeifer, R.N. Hardwick, W. Yue, P.W. Stewart, K.L.R. Brouwer, An experimental approach to evaluate the impact of impaired transport function on hepatobiliary drug disposition using Mrp2-deficient TR- rat sandwich-cultured hepatocytes in combination with Bcrp knockdown., Mol. Pharm. 11 (2014) 766–775. https://doi.org/10.1021/mp400471e.

[57]   H.U. Jeong, J.H. Kim, T.Y. Kong, W.G. Choi, H.S. Lee, Comparative metabolism of honokiol in mouse, rat, dog, monkey, and human hepatocytes,

Arch. Pharm. Res. 39 (2016) 516–530. https://doi.org/10.1007/s12272-016-0731-y.

[58] L. Zhu, G. Ge, Y. Liu, G. He, S. Liang, Z. Fang, P. Dong, Y. Cao, L. Yang, Potent and selective inhibition of magnolol on catalytic activities of UGT1A7 and 1A9, Xenobiotica. 42 (2012) 1001–1008. https://doi.org/10.3109/00498254.2012.681814.

[59] S.X. Yu, R.Y. Yan, R.X. Liang, W. Wang, B. Yang, Bioactive polar compounds from stem bark of Magnolia officinalis, Fitoterapia. 83 (2012) 356–361. https://doi.org/10.1016/j.fitote.2011.11.020.

[60] C.P. Yu, P.Y. Li, S.Y. Chen, S.P. Lin, Y.C. Hou, Magnolol and honokiol inhibited the function and expression of BCRP with mechanism exploration, Molecules. 26 (2021) 1–10. https://doi.org/10.3390/molecules26237390.

[61] J.H. Chen, K.F. Ke, J.H. Lu, Y.H. Qiu, Y.P. Peng, Protection of TGF-β1 against neuroinflammation and neurodegeneration in Aβ1-42-induced alzheimer's disease model rats, PLoS One. 10 (2015) 1–19. https://doi.org/10.1371/journal.pone.0116549.

[62] M. Maioli, V. Basoli, P. Carta, D. Fabbri, M.A. Dettori, S. Cruciani, P.A. Serra, G. Delogu, Synthesis of magnolol and honokiol derivatives and their effect against hepatocarcinoma cells, PLoS One. 13 (2018) 1–21. https://doi.org/10.1371/journal.pone.0192178.

[63] J. Shen, H. Ma, T. Zhang, H. Liu, L. Yu, G. Li, H. Li, M. Hu, Magnolol Inhibits the Growth of Non-Small Cell Lung Cancer via Inhibiting Microtubule Polymerization, Cell. Physiol. Biochem. 42 (2017) 1789–1801. https://doi.org/10.1159/000479458.

[64] S. Chei, H.J. Oh, J.H. Song, Y.J. Seo, K. Lee, B.Y. Lee, Magnolol Suppresses TGF-β-Induced Epithelial-to-Mesenchymal Transition in Human Colorectal Cancer Cells, Front. Oncol. 9 (2019) 1–11. https://doi.org/10.3389/fonc.2019.00752.

[65] H. Chen, W. Fu, H. Chen, S. You, X. Liu, Y. Yang, Y. Wei, J. Huang, W. Rui, Magnolol attenuates the inflammation and enhances phagocytosis through the activation of MAPK, NF-κB signal pathways in vitro and in vivo, Mol. Immunol. 105 (2019) 96–106. https://doi.org/10.1016/j.molimm.2018.11.008.

[66] Y.C. Cheng, M.J. Tsao, C.Y. Chiu, P.C. Kan, Y. Chen, Magnolol inhibits human glioblastoma cell migration by regulating N-cadherin, J. Neuropathol. Exp. Neurol. 77 (2018) 426–436. https://doi.org/10.1093/jnen/nly021.

[67] A.M. Ranaware, K. Banik, V. Deshpande, G. Padmavathi, N.K. Roy, G. Sethi, L. Fan, A.P. Kumar, A.B. Kunnumakkara, Magnolol: A neolignan from the Magnolia family for the prevention and treatment of cancer, Int. J. Mol. Sci. 19 (2018) 1–21. https://doi.org/10.3390/ijms19082362.

[68] N. Li, Y. Song, W. Zhang, W. Wang, J. Chen, A.W. Wong, A. Roberts, Evaluation of the in vitro and in vivo genotoxicity of magnolia bark extract, Regul. Toxicol. Pharmacol. 49 (2007) 154–159. https://doi.org/10.1016/j.yrtph.2007.06.005.

[69] Z. Liu, X. Zhang, W. Cui, X. Zhang, N. Li, J. Chen, A.W. Wong, A. Roberts, Evaluation of short-term and subchronic toxicity of magnolia bark extract in rats, Regul. Toxicol. Pharmacol. 49 (2007) 160–171. https://doi.org/10.1016/j.yrtph.2007.06.006.

[70] M. Li, F. Zhang, X. Wang, X. Wu, B. Zhang, N. Zhang, W. Wu, Z. Wang, H. Weng, S. Liu, G. Gao, J. Mu, Y. Shu, R. Bao, Y. Cao, J. Lu, J. Gu, J. Zhu, Y. Liu, Magnolol inhibits growth of gallbladder cancer cells through the p53

pathway, Cancer Sci. 106 (2015) 1341–13501. https://doi.org/10.1111/cas.12762.

[71] H.K. Han, L.T. Van Anh, Modulation of P-glycoprotein expression by honokiol, magnololand 4-O-methylhonokiol, the bioactive components of Magnolia officinalis, Anticancer Res. 32 (2012) 4445–4452. https://doi.org/32/10/4445 [pii].

[72] S. Di Micco, L. Pulvirenti, I. Bruno, S. Terracciano, A. Russo, M.C. Vaccaro, D. Ruggiero, V. Muccilli, N. Cardullo, C. Tringali, R. Riccio, G. Bifulco, Identification by Inverse Virtual Screening of magnolol-based scaffold as new tankyrase-2 inhibitors, Bioorganic Med. Chem. 26 (2018) 3953–3957. https://doi.org/10.1016/j.bmc.2018.06.019.

[73] L. Pulvirenti, V. Muccilli, N. Cardullo, C. Spatafora, C. Tringali, Chemoenzymatic Synthesis and α-Glucosidase Inhibitory Activity of Dimeric Neolignans Inspired by Magnolol, J. Nat. Prod. 80 (2017) 1648–1657. https://doi.org/10.1021/acs.jnatprod.7b00250.

[74] A. Baschieri, L. Pulvirenti, V. Muccilli, R. Amorati, C. Tringali, Chain-breaking antioxidant activity of hydroxylated and methoxylated magnolol derivatives: The role of H-bonds, Org. Biomol. Chem. 15 (2017) 6177–6184. https://doi.org/10.1039/c7ob01195d.

[75] J.F. Algorri, M. Ochoa, P. Roldán-Varona, L. Rodríguez-Cobo, J.M. López-Higuera, Photodynamic therapy: A compendium of latest reviews, Cancers (Basel). 13 (2021). https://doi.org/10.3390/cancers13174447.

[76] E.C. Aniogo, B. Plackal, A. George, H. Abrahamse, The role of photodynamic therapy on multidrug resistant breast cancer, Cancer Cell Int. 19 (2019) 1–14. https://doi.org/10.1186/s12935-019-0815-0.

[77] B.Q. Spring, I. Rizvi, N. Xu, T. Hasan, The Role of Photodynamic Therapy in Overcoming Cancer Drug Resistance., Photochem. Photobiol. Sci. (2015). https://doi.org/10.1039/C4PP00495G.

[78] H. Barr, C.J. Tralau, P.B. Boulos, A.J. MacRobert, R. Tilly, S.G. Bow, THE CONTRASTING MECHANISMS OF COLONIC COLLAGEN DAMAGE BETWEEN PHOTODYNAMIC THERAPY AND THERMAL INJURY, 46 (1987) 795–800.

[79] M.R. Hamblin, Photodynamic Therapy for Cancer: What's Past is Prologue, Photochem. Photobiol. 96 (2020) 506–516. https://doi.org/10.1111/php.13190.

[80] T.J. Dougherty, G.B. Grindey, R. Fiel, K.R. Weishaupt, D.G. Boyle, Photoradiation therapy. II. Cure of animal tumors with hematoporphyrin and light, J. Natl. Cancer Inst. 55 (1975) 115–121. https://doi.org/10.1093/jnci/55.1.115.

[81] M.E. Etcheverry, M.A. Pasquale, M. Garavaglia, Photodynamic therapy of HeLa cell cultures by using LED or laser sources, J. Photochem. Photobiol. B Biol. 160 (2016) 271–277. https://doi.org/10.1016/j.jphotobiol.2016.04.013.

[82] Q. Guo, B. Dong, F. Nan, D. Guan, Y. Zhang, 5-Aminolevulinic acid photodynamic therapy in human cervical cancer via the activation of microRNA-143 and suppression of the Bcl-2/Bax signaling pathway, Mol. Med. Rep. 14 (2016) 544–550. https://doi.org/10.3892/mmr.2016.5248.

[83] P. Mroz, A. Yaroslavsky, G.B. Kharkwal, M.R. Hamblin, Cell death pathways in photodynamic therapy of cancer, Cancers (Basel). 3 (2011) 2516–2539. https://doi.org/10.3390/cancers3022516.

[84]   S.M. Mahalingam, J.D. Ordaz, P.S. Low, Targeting of a Photosensitizer to the Mitochondrion Enhances the Potency of Photodynamic Therapy, ACS Omega. 3 (2018) 6066–6074. https://doi.org/10.1021/acsomega.8b00692.

[85]   D.J. Granville, J.G. Levy, D.W.C. Hunt, Photodynamic Treatment with Benzoporphyrin Derivative Monoacid Ring A Produces Protein Tyrosine Phosphorylation Events and DNA Fragmentation in Murine P815 Cells, Photochem. Photobiol. 67 (1998) 358–362.

[86]   R.R. Allison, Photodynamic therapy: Oncologic horizons, Futur. Oncol. 10 (2014) 123–142. https://doi.org/10.2217/fon.13.176.

[87]   O. Chepurna, I. Shton, V. Kholin, V. Voytsehovich, V. Popov, S. Pavlov, N. Gamaleia, W. Wójcik, M. Zhassandykyzy, Photodynamic therapy with laser scanning mode of tumor irradiation, Opt. Fibers Their Appl. 2015. 9816 (2015) 98161F. https://doi.org/10.1117/12.2229030.

[88]   Z. Huang, A review of progress in clinical photodynamic therapy, Technol. Cancer Res. Treat. 4 (2005) 283–293. https://doi.org/10.1177/153303460500400308.

[89]   A. Erkiert-Polguj, A. Halbina, I. Polak-Pacholczyk, H. Rotsztejn, Light-emitting diodes in photodynamic therapy in non-melanoma skin cancers - Own observations and literature review, J. Cosmet. Laser Ther. 18 (2016) 105–110. https://doi.org/10.3109/14764172.2015.1114635.

[90]   J. Neupane, S. Ghimire, S. Shakya, L. Chaudhary, V.P. Shrivastava, Effect of light emitting diodes in the photodynamic therapy of rheumatoid arthritis, Photodiagnosis Photodyn. Ther. 7 (2010) 44–49. https://doi.org/10.1016/j.pdpdt.2009.12.006.

[91]   S.L. Hopkins, B. Siewert, S.H.C. Askes, P. Veldhuizen, R. Zwier, M. Heger, S. Bonnet, An: In vitro cell irradiation protocol for testing photopharmaceuticals and the effect of blue, green, and red light on human cancer cell lines, Photochem. Photobiol. Sci. 15 (2016) 644–653. https://doi.org/10.1039/c5pp00424a.

[92]   O. Chepurna, A. Grebinyk, Y. Petrushko, S. Prylutska, S. Grebinyk, V. Yashchuk, O. Matyshevska, U. Ritter, T. Dandekar, M. Frohme, J. Qu, T.Y. Ohulchanskyy, LED-based portable light source for photodynamic therapy, (2019) 45. https://doi.org/10.1117/12.2541774.

[93]   O. Hasson, A. Wishkerman, CultureLED: A 3D printer-based LED illumination cultivation system for multi-well culture plates, HardwareX. 12 (2022) e00323. https://doi.org/10.1016/j.ohx.2022.e00323.

[94]   E.C. Lins, C.F. Oliveira, O.C.C. Guimarães, C.A.D.S. Costa, C. Kurachi, V.S. Bagnato, A novel 785-nm laser diode-based system for standardization of cell culture irradiation, Photomed. Laser Surg. 31 (2013) 466–473. https://doi.org/10.1089/pho.2012.3310.

[95]   K. Zhang, M. Waguespack, E.M. Kercher, B.Q. Spring, An automated and stable LED array illumination system for multiwell plate cell culture photodynamic therapy experiments, Res. Sq. Preprint (2022) 1–18.

[96]   E.N. de Gálvez, J. Aguilera, P. Fonda-Pascual, M.V. de Gálvez, J.R. de Andrés-Díaz, S. Vidal-Asensi, E. Herrera-Acosta, A. Gago-Calderon, Analysis and evaluation of the operational characteristics of a new photodynamic therapy device, Photodiagnosis Photodyn. Ther. 37 (2022) 0–7. https://doi.org/10.1016/j.pdpdt.2022.102719.

RESEARCH OBJECTIVES

- Study of magnolol derivatives as ABCG2 inhibitors.

  - Screening of magnolol derivatives as ABCG2 inhibitors on stably transfected cell line;
  - Verify the selectivity of magnolol derivatives on P-gp activity;
  - Determine the IC_{50} value of ABCG2 inhibition by flow cytometry;
  - Determine the IG_{50} value by MTT cytotoxicity assay;
  - Verify the transport of magnolol derivatives by ABCG2;
  - Determine the therapeutic ratio and identify the most promising compound;
  - Verify possible effects of magnolol derivatives binding on ABCG2 using membrane-based approaches: ATPase activity and thermostability;
  - Verify the ability of magnolol derivatives to inhibit the ABCG2-mediated efflux of different substrates;
  - Determine the impact of magnolol derivatives on mRNA expression levels of ABCG2;
  - Verify the conformational changes using 5D3 binding assay;
  - Determine the type of inhibition;
  - Verify the interactions between magnolol derivatives and ABCG2 by molecular docking.

- In-house development of a LED-based photodynamic therapy device for *in vitro* assays

  - Construction of the prototype with unexpensive and commercially available material and components;
  - Codding of operational system through free platforms;
  - Create a decision flowchart to support setup and operation of the prototype;
  - Verify the sensitization enhancement of a tumoral cell line through photodynamic therapy utilizing a photosensitizer and the prototype as irradiation source;
  - Verify the association between photosensitization performed by the prototype and ROS generation increase;
  - Compare the results obtained with the prototype and a commercial LED-based device.

CAPTHER 1 – MAGNOLOL DERIVATIVES AS SPECIFIC, UNTRANSPORTED, AND NONCYTOTOXIC INHIBITORS OF ABCG2 TRANSPORTER

Manuscript to be submitted in the journal Chemico-Biological Interactions

Isadora da Silva Zanzarini[1], Diogo Henrique Kita[1,2], Larissa de Oliveira Prado[1], Gustavo Scheiffer[1], Kelly Karoline dos Santos[1], Julia de Paula Dutra[1], Vivian Rotuno Moure[1], Fabiane Gomes de Moraes Rego[3], Geraldo Picheth[3], Suresh V. Ambudkar[2], Corrado Tringali[4], Vera Muccilli[4] and Glaucio Valdameri[1]

[1]Pharmaceutical Sciences Graduate Program, Laboratory of Cancer Drug Resistance, Federal University of Parana, Curitiba, Brazil

[2]Laboratory of Cell Biology, Center for Cancer Research, National Cancer Institute, National Institutes of Health, Bethesda, MD, USA

[3]Department of Clinical Analysis, Federal University of Parana, Curitiba, Brazil

[4]Department of Chemical Sciences, University of Catania, Catania, Italy

Correspondence: G. Valdameri, Pharmaceutical Sciences Graduate Program, Laboratory of Cancer Drug Resistance, Federal University of Parana, Rua Prefeito Lothario Meissner, 632, Jardim Botânico, Curitiba, PR 80210-170, Brazil

1 INTRODUCTION

Multidrug resistance (MDR) related to cancer has been described as a major challenge in oncological therapy [1]. Among several biological mechanisms of MDR, the overexpression of ATP-binding cassette (ABC) transporters is considered the leading cause of drug resistance development in neoplastic cells [2]. These overexpressed ABC transporters increase the efflux of chemotherapeutic drugs, decreasing intracellular accumulation to subclinical concentrations, leading the protocols to their failure [3]. ABC transporters are described as polyspecific due to their ability to export, in eukaryotic cells [4], a wide range of drugs with unrelated chemical structures and cellular targets [5]. The human genome codes for 48 ABC proteins [6] and among them, three ABC transporters are closely involved with the MDR phenotype: glycoprotein-P (P-gp or MDR1), multidrug resistance protein 1 (MRP1) and breast cancer resistance protein (BCRP or ABCG2) [7].

The use of ABC transporters inhibitors is the most common strategy to overcome MDR. The first identified ABC transporter related to MDR was P-gp [8], nevertheless, clinical studies of P-gp inhibitors are still failing to improve the chemotherapeutic efficacy of oncological protocols [9–12]. One of the diverse reasons for the reported clinical failure is the fact that many drugs transported by P-gp are also transported by ABCG2 and other ABC transporters [13]. Since P-gp and ABCG2 are both overexpressed in several cancers, and despite recent advances, there are very few potent, non-toxic ABCG2 inhibitors available for clinical studies, demonstrating that the development of new ABCG2 inhibitors is an urgent necessity. During the last few years we have identified certain classes of compounds as potent ABCG2 inhibitors, including chromones [14,15], stilbenes [16], chalcones [17], indeno[1,2-*b*]indoles [18–20] and porphyrins [21].

Natural products are a great source of chemical scaffolds for new drugs and represent a powerful starting point for ABCG2 inhibitors. Flavonoids [22], botryllamides [23], polyphenols [24] are among the natural compounds identified as inhibitors of ABCG2 that were latter modified to improve their activity. Among the most widely researched polyphenols, two compounds have shown numerous and increasing research data in recent years: magnolol and its isomer honokiol, which have a biphenolic nucleus with two allylic side chains [25].

Numerous preclinical studies have verified an antitumoral activity exerted by magnolol against different types of cancer, such as lung, prostate, breast, gallbladder, colon, skin and liver [26–32]. *In vitro* and, subsequently, *in vivo* studies have shown that magnolol has a satisfactory safety profile [33,34], contributes to the reduction of tumor growth, induces apoptosis and inhibits invasion, migration and metastasis [32,35,36].

Some magnolol derivatives, synthesized through chemical replacements and/or insertions in the main core structure showed inhibitory activities against tankyrase-2 [37] and yeasts α-glucosidase enzymes. The latter is also a promising property when considering the optimized development of new antidiabetic drugs [38].

Additionally, studies suggest that magnolol, honokiol and 4-O-methylhonokiol may be promising agents in combating MDR through down-regulation of P-gp (ABCB1) expression levels [39]. More recently, the two isomers were described as promising inhibitors of ABCG2 activity and down-regulators of expression levels [40]. In this study, further structural insights on magnolol main scaffold led us to synthesize new

derivatives and the mechanism of ABCG2 inhibition of the most promising compound were characterized.

2 MATERIAL AND METHODS

2.1 CHEMICALS

Magnolol derivatives were synthesized by the research group of Corrado Tringali and Vera Muccilli (University of Catania, Italy). The compounds were dissolved in DMSO (Sigma-Aldrich®) and the stock solutions stored at -20°C and thawed at the time of use.

2.2 CELL LINES AND CULTURES

The human fibroblast HEK293 cell line was stably transfected with plasmid (pcDNA3) coding for human ABCG2 (HEK293-*ABCG2*) as previously described [41]. The murine fibroblast NIH3T3 drug-resistant cell line was stably transfected with retroviral vector (MDR1/A-G185) coding for NIH3T3/*ABCB1* as previously described [42]. Both parental and stably transfected HEK293 and NIH3T3 cell lines were kindly provided by Dr. Attilio Di Pietro (IBCP, Lyon, France). All cell lines were cultivated in High Glucose modified Dulbecco's Modified Eagle Medium), supplemented with 10% fetal bovine serum (FBS), 1% penicillin/streptomycin and maintained at 37 °C and 5% CO_2 under controlled humidity. The stably transfected cells were additionally treated with either 0.75 mg mL^{-1} of G418 (HEK293-*ABCG2*) or 60 ng mL^{-1} of colchicine (NIH3T3-*ABCB1*). The cells were cultivated until reaching 80-90% of confluence and then used for experimentation.

2.3 TRANSPORT ASSAY

Transport assay was carried out with cells overexpressing the ABC transporters: HEK293-*ABCG2* and NIH3T3-*ABCB1* (P-gp). Cells were seeded at the density of 1.5×10^5 cells/well in 24 well culture plates and incubated for 48 h at 37 °C under 5% CO_2. Cells were treated with magnolol derivatives at 10 or 50 µM and substrate (5 µM of mitoxantrone or rhodamine 123 for ABCG2 and P-gp, respectively). Stably transfected cells treated with reference inhibitors Ko143 (0.5 µM) and GF120918 (0.5 µM) were used as positive controls of inhibition for ABCG2 and P-gp, respectively. Negative control consisted of stably transfected cells exposed only to

their respective substrates. Cells in all conditions (negative/positive controls and tested conditions) were incubated for 30 min at 37 °C and 5% CO2. After treatment, cells were washed with PBS (400 µl), detached with trypsin (50 µl) and resuspended in ice cold PBS (300 µl). The intracellular fluorescence was monitored with a FACS Calibur cytometer (Becton Dickinson) using Red Laser/FL4 channel for mitoxantrone and Blue Laser/FL1 channel and rhodamine 123, with at least 10,000 events collected inside the gate (geometrical delimitation of higher density and most homogeneous cells within a dot plot). The maximal fluorescence (assumed as 100%) was determined by the median value of intracellular accumulation of substrates in stably transfected cells incubated with their specific reference inhibitors (or using their respective wild-type cell lines). A minimum ratio of 2 between the maximum and minimum fluorescence values obtained by the positive and negative inhibition controls, respectively, was necessary to validate each experiment. The percentage of transport inhibition was calculated by the following equation:

$$\% \ inhibition \ = \ (C - S)/(I - S) \ \times 100$$

where "C" corresponds to the intracellular fluorescence of cells in the presence of the tested compounds and their specific substrates, "S" corresponds to the intracellular fluorescence of cells in the presence of substrate alone, and "I" corresponds to the intracellular fluorescence of cells in the presence of both their specific substrates and reference inhibitors. The IC_{50} curves of ABCG2 inhibition were obtained with increasing concentrations of magnolol derivatives (0.39 µM–50 µM, 30 minutes of incubation) using mitoxantrone as fluorescent substrate.

2.4 CONFOCAL MICROSCOPY

HEK293-*ABCG2* cells were seeded at a density of $1x10^5$ cells/well in 24-well culture plates containing coverslips for microscopy and incubated for 48 h at 37 °C under 5% CO_2. Cells that adhered to the coverslips were treated with 50 µM of inhibitor and 1 µM of Hoechst 33342 for 30 min at 37 °C and 5% CO_2. After incubation, the coverslips were removed from the plate and placed on slides for microscopy. The slides were then read in a confocal microscopy Nikon A1R MP + (NIKON, Tokyo, Japan) using an oil-immersed 40X objective (with the numerical aperture of 1.15). A laser of 405 nm was used for excitation and the fluorescence emission was recorded

using a bandpass filter of 425–475 nm. The software Nis Elements 4.20 (NIKON, Tokyo, Japan) was used for visualization of the images.

2.5 CELL VIABILITY ASSAY

Cell viability was evaluated with a 3-(4,5-dimethylthiazol-2-yl)-2,5-iphenyltetrazolium bromide (MTT) colorimetric assay [43]. HEK293 wild type (WT) and HEK293-*ABCG2* cells were seeded into 96-well culture plates at 1.5×10^4 cells/well density. After overnight incubation, the cells were treated with various concentrations of magnolol derivatives (0.19 – 100 µM) for 72 h at 37 °C under 5% CO_2. After the treatment, the culture medium was removed and 100 µL of a 0.5 mg. mL^{-1} of MTT solution was added. Cells were then incubated for 4 h at 37 °C under 5% CO_2. The formazan crystals were dissolved with a solution of DMSO/ethanol (1:1) and the absorbance was measured at 570 nm using a Multiscan FC microplate reader (Thermo Scientific). The results were expressed as percentage of viable cells versus control cells (0.1% DMSO, v/v) taken as 100%.

2.6 mRNA EXPRESSION LEVELS BY qPCR

Total RNA was obtained of HEK293-*ABCG2* cells from cultures with approximately 90% of confluence after treatment for 72 h with CT_M15 (50 µM). The total RNA isolation was performed using TRIzol (Invitrogen) protocol according to the manufacturer's instructions. A NanoDrop™ Spectophotometer was used to quantify RNA concentration and the integrity was evaluated by 1% agarose gel electrophoresis and, subsequently, RNA was stored at -80 °C. Two micrograms of total RNA were reverse transcribed using High Capacity cDNA Reverse Transcription Kit (Applied Biosystems) according to the manufacturer's instructions, and the resulting cDNA was stored at -20 °C. Using cDNAs as the template, quantitative real-time PCR (qPCR) was performed using the SYBR Green PCR Master Mix (Applied Biosystems) in a 7500™ Real-Time PCR Detection System (Applied Biosystems). A dissociation cycle was performed after each run to check for non-specific amplification or contamination. The mRNA expression levels were normalized using the geNorm 3.4 software, and the corresponding housekeeping gene expression levels. Sets of specific primers were designed using Primer designing tool - NCBI and validated through BLAST and BLAT, and their respective sequences are shown in Table 1. Relative expression levels were estimated using the method described by Pfaffl [44].

TABLE 1 - NUCLEOTIDE SEQUENCES OF PRIMERS USED FOR qPCR.

Gene	NCBI reference	Sequence	Reference
PPIA	NM_021130.5	F- TAAAGCATACGGGTCCTGGC R- TGCCATCCAACCACTCAGTC	[45–48]
RPS13	NM_001017.3	F- CGTCCCCACTTGGTTGAAGT R- TGAATCTCTCAGGATTACACCGA	[46,49]
HPRT1	NM_000194.3	F- CAGGGATTTGAATCATGTTTGTGT R- ACTCCAGATGTTTCCAAACTCAAC	[45,50,51]
ABCG2	NM_001257386.2	F - ATGGTCTGTTGGTCAATCTCAC R – TTATGCTGCAAAGCCGTAAATCC	This work

2.7 ATPase ASSAY

The ATPase activity was determined as previously described [52]. High-Five insect cell total membranes overexpressing ABCG2 were used at a concentration of 5 µg protein/tube in a final volume of 100 µL. The membranes were incubated in assay buffer with the following composition: 50 mM Tris–HCl, pH 6.8, 150 mM N-methyl-D-glucamine (NMDG)-Cl, 5 mM sodium azide, 1 mM EGTA, 1 mM ouabain, 2 mM DTT, and 10 mM $MgCl_2$, in the presence or absence of sodium orthovanadate (0.3 mM). The protein-buffer mix was treated with the inhibitor at increasing concentrations (0 – 50 µM) and incubated for 20 min at 37 °C in the presence of ATP (5 mM). The reaction was stopped with the addition of 100 µL of 5% SDS, 400 µL of Pi solution (sulfuric acid 36.2 N, water, ammonium molybdate and antimony potassium tartrate) and 200 µL of 1% ascorbic acid. After 10 min, the absorbance was measured at 880 nm using Ultrospec 3100 pro spectrophotometer (Amersham Biosciences, UK).

2.8 CONFORMATIONAL ANTIBODY BINDING (5D3)

HEK293-*ABCG2* cells were seeded at a density of 2×10^5 cells/well in 24 well culture plates and incubated for 48 h at 37 C under 5% CO_2. After incubation the cells were washed with PBS, detached by trypsin, collected with 300 µL of PBS and centrifuged (1000×g for 3 min). The cell pellet was resuspended in 100 µL of PBS containing 4 µL of a BSA solution (1 mg/mL). Cells were treated with inhibitor at 50 µM for 10 min at 37 C. The 5D3 primary antibody (Purified mouse anti-human CD338, BD Pharmigen—1:100) was added and incubated at 37 °C for 30 min. After incubation, centrifugation was performed at 1000×g for 3 min and the cell pellet was resuspended

in 100 µL of PBS containing the secondary antibody conjugated with phycoerythrin (PE Goat anti-mouse IgG, Abcam—1:200) and incubated at 37 °C for 30 min. After incubation, centrifugation was performed at 1000×g for 3 min and the pellet resuspended in 300 µL of ice-cold PBS. The flow cytometry analysis was performed as previously described, with a FACS Calibur cytometer (Becton Dickinson) using the blue laser (488 nm) and FL-2 filter.

2.9 THERMOSTABILITY ASSAY

The thermal stability assay was performed as previously described [53]. Total membrane prepared from High Five insect cells overexpressing ABCG2 at were incubated (3 µg protein/tube) with assay buffer with the following composition: 50 mM Tris–HCl, pH 6.8, 150 mM N-methyl-d-glucamine (NMDG)-Cl, 5 mM sodium azide, 1 mM ouabain and 2 mM DTT, in the presence or absence of 0.3 mM orthovanadate at final volume of 50 µL. To evaluate the effect of CT_M15 over thermal stability, each sample was prepared with 12.5 mM $MgCl_2$ or 6.25 mM ATP and incubated with a temperature range from 37 to 71 °C for 10 min using a thermocycler C1000 Touch (Bio-Rad, Hercules, CA). After incubation, 10 µL of 25 mM ATP or 50 mM $MgCl_2$ (5 and 10 mM final concentration, respectively) was added and incubated at 37 °C/20 min to allow ATP hydrolysis. The reaction was stopped with the addition of 50 µL of Pi solution containing 1% ammonium molibdate, 2.5 N H_2SO_4 and 0.014% potassium-antimony tartrate. To evaluate the absorbance, the samples were transferred to a 96 well plate (50 µL/well) and added 150 µL of 0.33% sodium ascorbate solution. The absorbance was measured after 15 min of incubation at room temperature using the microplate reader Spectramax iD3 (Molecular Devices, San Jose, CA). The sensitive activity to vanadate (Vi) was calculated as the difference between the activity in the absence of Vi and the activity in the presence of Vi to each temperature.

2.10 MOLECULAR MODELLING

Molecular docking studies were performed using the ABCG2 structure deposited in the Protein Data Bank under the ID code 6VXI. The inhibitors were structurally optimized by applying the Mopac 2016 program (MOPAC2016, James J. P. Stewart, Stewart Computational Chemistry, Colorado Springs, CO, USA, http://OpenMOPAC.net (2016) by using the PM7 method [54]. The structures for ABCG2 and inhibitors were prepared for use with AutoDock Vina [55] using AutoDock

Tools (v.1.5.6). For molecular docking, an area of 40 × 40 × 40 Å and coordinates X= -0.181, Y= -0.222 and Z= 0.571 was delimited. Two strategies were used: first, docking on the apo protein and then docking on the structure containing the mitoxantrone molecule, in the position defined by the original file (Cryo-EM). The exhaustiveness parameter was set to 75 and a maximum number of 20 binding modes was used. Docked models of the inhibitors, binding sites and amino acid interactions were visualized with ABCG2 using PYMOL (Molecular Graphics System, Version 1.3, Schrödinger, LLC) and Maestro, the latter being used to determine the intermolecular interactions between the molecules and the side chains of the transporter.

3 RESULTS

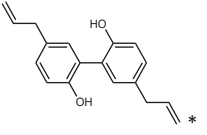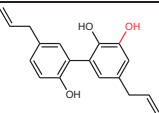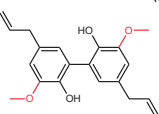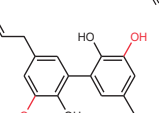### 3.1 IDENTIFICATION OF CT_M15 AS A SELECTIVE AND NONCYTOTOXIC ABCG2 INHIBITOR
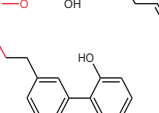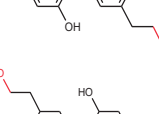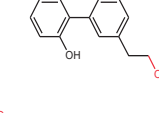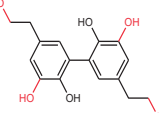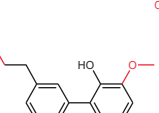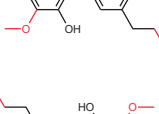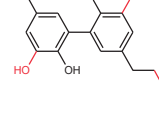
A total of 13 magnolol derivatives (Table 2) were evaluated as potential inhibitors of ABCG2 transporter by examining their effect on mitoxantrone ABCG2-mediated efflux. Stably transfected cells overexpressing ABCG2 (HEK293-*ABCG2*) were incubated with the compounds at concentrations of 10 µM and 50 µM for 30 min. The intracellular fluorescence of mitoxantrone was monitored by flow cytometry. One magnolol derivative (CT_M10) showed a partial inhibition (~50% of inhibition) at the higher concentration tested. Only CT_M15 showed a total inhibition of mitoxantrone ABCG2-mediated efflux (Table 2).
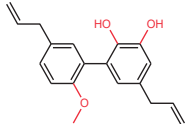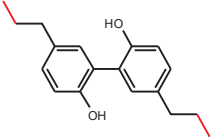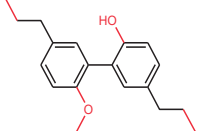
The series of compounds comprehends results of chemical reactions such as insertions and replacements of one or two phenolic nucleus as well saturations, insertions, and replacements of their side chains. The chemical alterations did not follow a pattern on ABCG2 inhibition, since the two best compounds are dramatically different: CT_M10 presents two insertions on its biphenolic scaffold (hydroxylation and methoxylation) and also bears saturated and esterified aliphatic chains; CT_M15 presents a very similar structure when compared to its precursor magnolol, admitting only one replacement in one phenolic nucleus (methoxylation).

Additionally, the selectivity toward ABCG2 was evaluated comparing the effect of magnolol derivatives on P-gp activity using rhodamine 123 as fluorescent substrate. Stably transfected cells overexpressing P-gp (NIH3T3-*ABCB1*) were used. As shown in Table 2, all compounds selectively inhibited ABCG2 activity since they did not show

any inhibition of P-gp. These results suggest that magnolol derivatives are a class of compounds that exclusively affects the activity of ABCG2 transporter.

TABLE 2 - SCREENING OF MAGNOLOL DERIVATIVES ON ABC TRANSPORTERS (ABCG2 AND P-GP)

	Compound	Inhibition (% ± SD)			
		ABCG2		ABCB1 (P-gp)	
		10 µM	50 µM	10 µM	50 µM
	CT_M1	2.5 ± 3.6	6.9 ± 3.8	-0.3 ± 2.0	-0.3 ± 2.8
	CT_M3	6.1 ± 7.9	12.8 ± 13.2	-0.8 ± 2.0	0.0 ± 2.4
	CT_M4	0.6 ± 2.0	1.0 ± 0.5	0.4 ± 1.9	-1.0 ± 2.0
	CT_M5	0.9 ± 2.7	3.6 ± 2.8	-0.3 ± 2.0	-0.5 ± 1.5
	CT_M6	10.1 ± 2.7	21.9 ± 3.4	0.0 ± 1.2	-0.1 ± 1.6
	CT_M7	0.1 ± 1.8	2.7 ± 0.5	0.0 ± 2.3	-0.3 ± 1.6
	CT_M9	7.0 ± 2.1	21.5 ± 4.7	0.3 ± 0.6	-0.4 ± 1.3
	CT_M10	21.8 ± 12.0	53.1 ± 8.5	-0.6 ± 1.4	-0.4 ± 1.6
	CT_M15	62.0 ± 11.9	105.4 ± 13.8	-0.7 ± 1.2	2.8 ± 3.8
	CT_M16	5.9 ± 10.9	32.8 ± 5.5	-1.1 ± 1.5	-0.5 ± 2.1

	CT_M19	4.0 ± 4.4	19.5 ± 4.4	1.1 ± 4.6	-1.2 ± 1.8
	CT_M20	1.8 ± 1.7	19.5 ± 4.5	0.5 ± 0.9	-6.4 ± 0.3
	CT_M21	1.1 ± 5.4	20.4 ± 1.7	0.2 ± 0.8	2.0 ± 1.9

*Chemical structure of magnolol, the common scaffold of magnolol derivatives studied in this work.

HEK293-*ABCG2* and NIH3T3-*ABCB1* cells were exposed to mitoxantrone (5 µM) and rhodamine 123 (5 µM) respectively, and magnolol derivatives (10 and 50 µM). Ko143 (0.5 µM) and GF120918 (0,5 µM) were used as positive controls, which produce 100% inhibition, for ABCG2 and P-gp, respectively. Intracellular accumulation of the fluorescent substrates was monitored by flow cytometry using FL4-H (ABCG2) and FL1-H (P-gp) channels. Results were expressed as percent of inhibition related to positive controls. The data represents the mean ± SD of, at least, three independent experiments.

The effect of the two most promising magnolol derivatives on ABCG2 function was explored by different approaches. HEK293-*ABCG2* cells were submitted to a short-term (30 min) treatment using increasing concentrations of CT_M10 and CT_M15 to determine the IC_{50} values (concentration that produce the half-maximal inhibition). CT_M10 and CT_M15 showed IC_{50} values of ABCG2 inhibition of 22.6 (Fig. 1A) and 9.8 µM (Fig. 1B), respectively. In addition, these data revealed that CT_M15 is a total ABCG2 inhibitor, such as the reference inhibitor Ko143 (Fig. 1C).
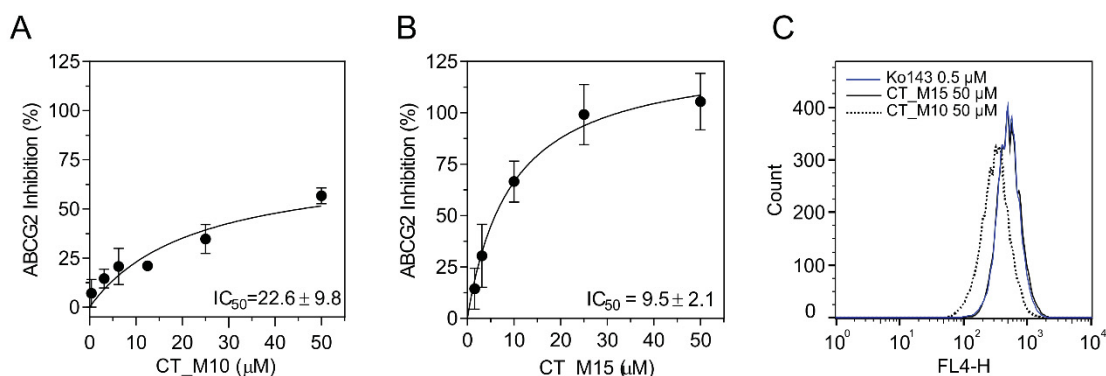
Figure 3. Inhibition curves of magnolol derivatives and histogram overlays. IC_{50} curves of ABCG2 inhibition for CT_M10 (A) and CT_M15 (B). Cells HEK293-*ABCG2* were exposed to mitoxantrone (5 µM) and magnolol derivatives (CT_M10 and CT_M15 at 0.039 - 50 µM). Ko143 (0.5 µM) was used as positive control (100% inhibition). Results were expressed as percent of inhibition relate to the positive control. (C) Histograms of ABCG2 inhibition: CT_M10, CT_M15 and Ko143.

The cytotoxicity profile comparing the effect of drugs in parental cells and cells overexpressing the target ABC transporter can provide valuable information about a possible ABCG2-mediated cross-resistance or collateral sensitivity [56]. HEK293 wild type and HEK293-*ABCG2* cells were submitted to a long-term (72 hours) treatment of increasing concentrations of CT_M10 and CT_M15 (Fig. 2). CT_M10 was cytotoxic at high concentrations, and the similar cytotoxicity pattern for both cell lines suggests an absence of cross-resistance, that means that CT_M10 is not recognized as an ABCG2 substrate (Fig. 2A). In addition, CT_M15 did not showed a cytotoxic effect even at high concentrations (Fig. 2B).

Considering the two most important parameters for identification of new ABCG2 inhibitors, potency of inhibition and intrinsic cell cytotoxicity, the therapeutic ratio (TR) values were calculated as the ratio between the IG_{50} value (concentration that reduces 50% of the cell viability) and IC_{50} value. As shown in figure 2C, CT_M15 was the best compound, showing a TR almost ten times greater than CT_M10.

Together, these data highlights that CT_M15 is the most promising compound from this series. Those values are still very low when compared to TR of other ABCG2 inhibitors, such as the value of 300-400 (IC_{50} = 0.05-0.1 µM and IG_{50} = 18-34 µM) in the case of Ko143 [57,58].
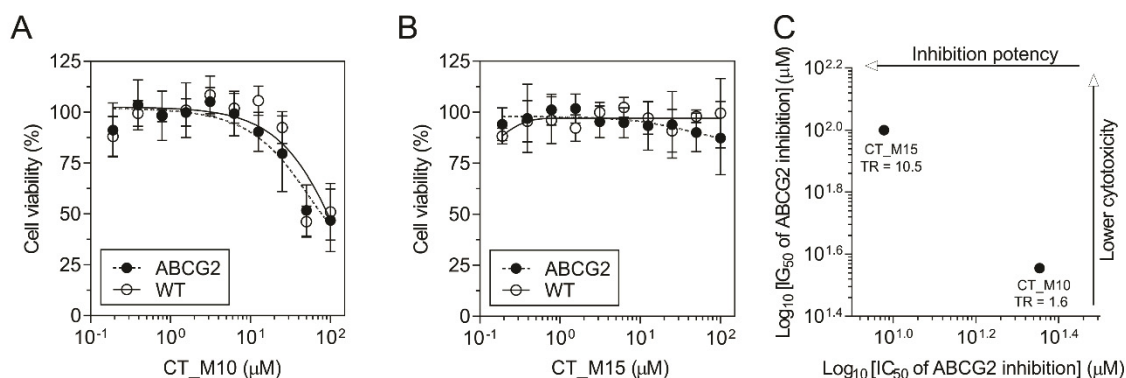
Figure 4 - Cell viability assay and TR representation. Cytotoxic profile of the two best compounds, CT_M10 (A) and CT_M15 (B). HEK 293-*ABCG2* and HEK293 wild-type cells were submitted at a long-term treatment (72 hours) with increasing concentrations of magnolol derivatives (0.19 - 100 µM). (C) Inhibition potency and cytotoxicity of the compounds with their respective therapeutic ratios.

3.2 STUDY OF CT_M15 ON ABCG2 USING MEMBRANE-BASED APPROACHES

Substrates and inhibitors of ABCG2 commonly exert opposite effects on its ATPase activity, inhibiting and stimulating it, respectively [59,60]. The effect of CT_M15 on the ABCG2 ATPase activity was studied using total membranes from High-Five insect cells overexpressing the ABCG2 transporter. As shown in Fig. 3A, this magnolol derivative triggered a dual effect, stimulating the ABCG2 ATPase activity of ABCG2 (~60%) at low concentrations and inhibiting (~30%) at the higher concentration (50 µM). This dual behavior concentration-dependent was also described for other ABCG2 inhibitors, such as nilotinib [61] and gefitinib [62].

Additionally, the effect of CT_M15 on thermostability of the protein was studied in membranes of insect cells overexpressing ABCG2. The thermostability of a protein is often altered due to conformational changes induced by a ligand [63]. To study the binding of CT_M15 on ABCG2 and possible allosteric conformational changes, a thermostability assay in the presence and absence of ATP was performed. Interestingly, CT_M15 decreased the IT_{50} values compared to the control (DMSO) (Fig.

3B and C), suggesting that the binding of this magnolol derivative destabilize the protein structure.
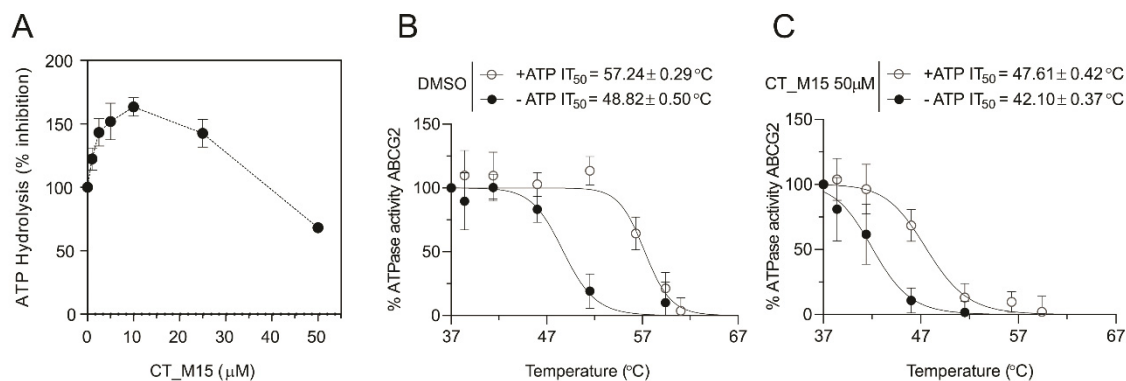
Figure 5 - Effects of CT_M15 on ABCG2 ATPase activity and protein thermostability. (A) Effect of CT_M15 at increasing concentrations (0.001 – 50 μM) on basal ABCG2 ATPase activity. Thermostability assay in the absence (B) and the presence (C) of CT_M15. The data represent mean ± SD of three independent experiments performed in duplicate.

3.3 STUDY OF CT_M15 ON ABCG2 USING CELL-BASED APPROACHES

To additionally characterize the mechanism of inhibition caused by CT_M15, the functional inhibition was studied using other substrate of ABCG2. The intracellular fluorescence of Hoechst 33342 was analyzed by confocal microscopy. The results were compared with the effect caused by the reference inhibitor Ko143. A diffuse fluorescent pattern was observed in the absence of inhibitors (Fig. 4A). Whereas, similarly to Ko143, CT_M15 promoted an increase in the intracellular levels of Hoechst 33342 (Fig. 4A), confirming that CT_M15 is not a substrate-specific inhibitor.

To further explore the mechanism of inhibition, the effect of CT_M15 on mRNA ABCG2 expression levels was studied by qPCR. As shown in figure 4B, CT_M15 did not significantly affected the transcriptional levels of ABCG2, suggesting that this compound is not a ABCG2 modulator, but a functional ABCG2 inhibitor. In addition, the effect of CT_M15 on protein conformation was investigated by the 5D3 shift assay. This assay consists in the use of the conformational antibody 5D3, which recognizes an epitope in the extracellular loop of ABCG2. As shown in Fig. 4C and D, the magnolol derivative triggered an increase of 5D3 binding similar to the reference inhibitor Ko143, suggesting that CT_M15 interaction causes important conformational changes in the extracellular region of the transporter.

The absence of ABCG2-mediated transport of CT_M15 suggests that this magnolol derivative does not share the same binding region or site with ABCG2 substrates. To pursue this hypothesis, the type of inhibition was investigated using increasing concentrations of both mitoxantrone and CT_M15. The data showed an increasing of Vmax and Km while inhibitor concentration increased, suggesting a mixed type of inhibition, which can be visualized by the Lineweaver-Burk plot (Fig. 4E).
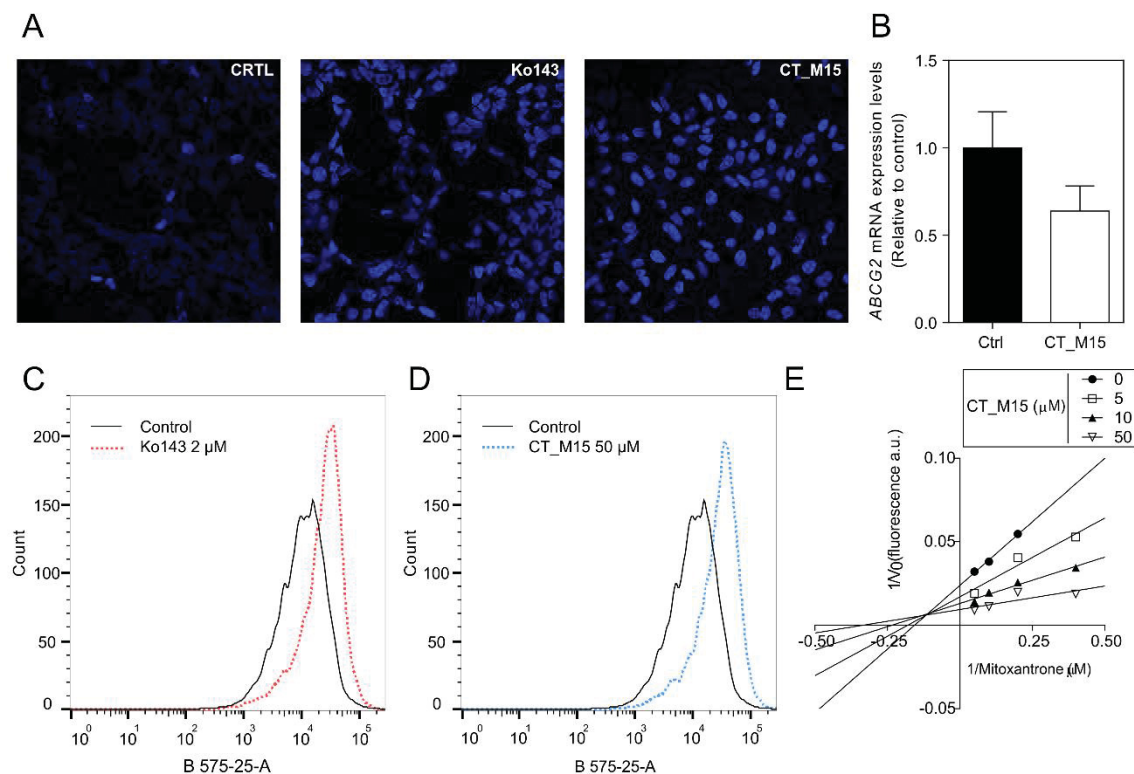
Figure 6 - ABCG2 inhibition, mRna expression levels, 5D3 shift assay and type of inhibition. (A) Intracellular accumulation of Hoechst 33342 (1 µM) in HEK293-*ABCG2* cells by confocal microscopy. Ko143 (0.5 µM) was used as control. CT_M15 was tested at 50 µM. Histograms from the conformational 5D3 antibody shift assay. (B) Impact of CT_M15 on mRNA expression levels. Overlay of untreated control and cells treated with Ko143 2 µM (C) and CT_M15 50 µM (D). (E) Lineweaver-Burk plot using different concentrations of CT_M15 and mitoxantrone.

3.4 STUDY OF CT_M15 ON ABCG2 USING AN *IN SILICO* APPROACH

To further understand the binding of CT_M15 on ABCG2 and the mechanism of inhibition, a molecular docking study was conducted following two strategies: first, using the apo protein in which the substrate was removed, and the second using the structure containing the mitoxantrone molecule, in the position obtained by Cryo-EM.

To compare the binding of CT_M15 on ABCG2, the inactive analogue CT_M16, that contains a second methoxy group instead of a hydroxy group was used. Docking analysis using the ABCG2 apo structure revealed an overlap of the binding site for CT_M15 and CT_M16 (Fig. 5A). A very similar behavior of both molecules was observed, both CT_M15 and CT_M16 bound with identical conformations, preferentially to the central pocket of drug binding site (drug binding cavity). In addition, the docking analysis revealed that both molecules were stabilized through hydrophobic

interactions with the F439 residues of the A and B chains (Fig. 5A), as observed for mitoxantrone (MTX) alone (Fig. 5C).

Interestingly, the docking analysis using the ABCG2 structure containing the substrate MTX revealed a shift of the CT_M15 and CT_M16 binding sites (Fig. 5B). This shift was more evident in the case of CT_M15 when compared with CT_M16. This different binding sites in presence of the substrate could explain why CT_M15 inhibit the ABCG2 transport activity while CT_16 showed a mild inhibitory effect. In addition, no specific intermolecular interactions were identified in the docking of the structure in the presence of MTX. Finally, the different binding sites of CT_M15 and MTX supports the mixed type of inhibition observed by this inhibitor.
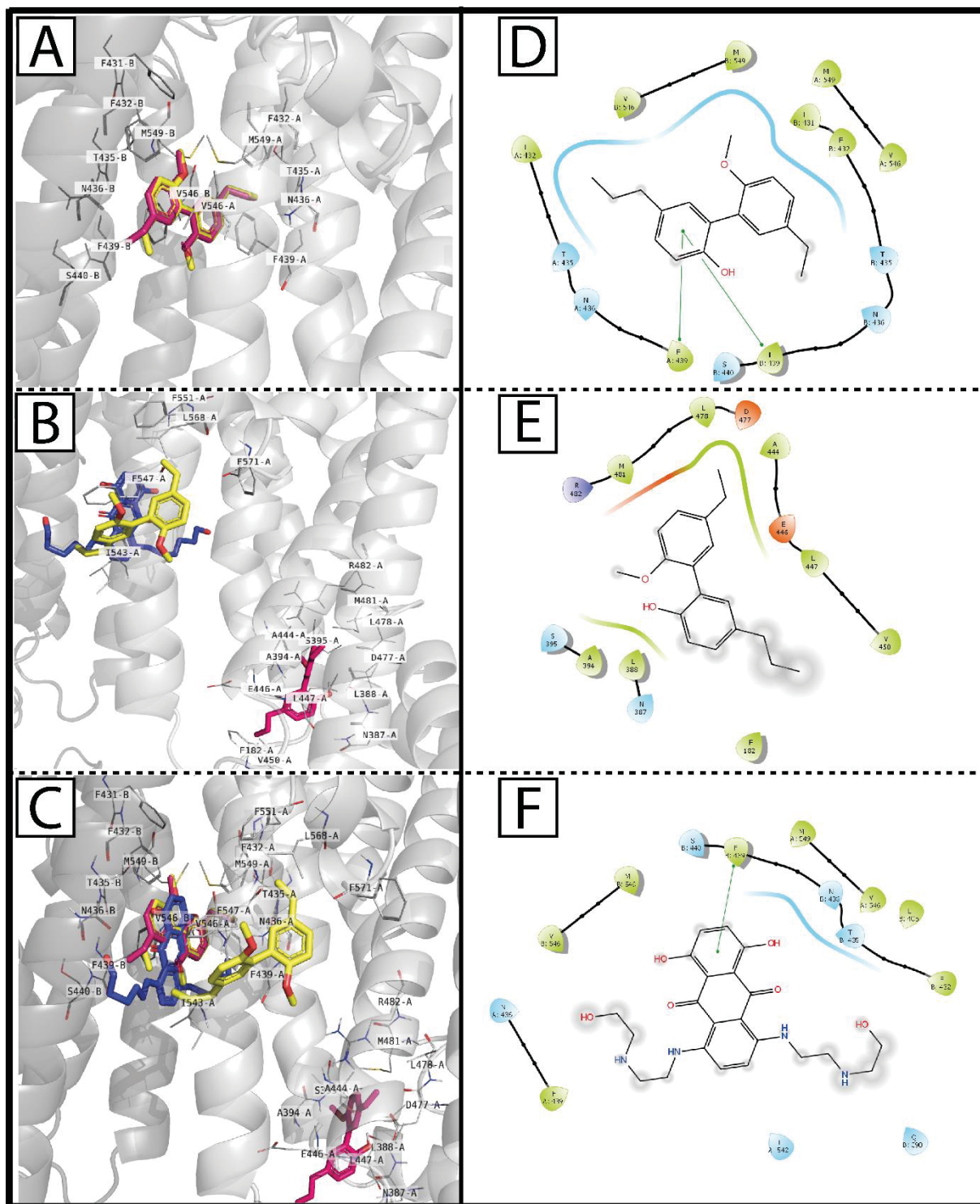
Figure 7 - Docking of CT_M15, CT_M16 and mitoxantrone on ABCG2. Binding site of CT_M15 (in pink) and CT_M16 (in yellow) on ABCG2 structure (PDB: 6VXI). (A) ABCG2 structure without mitoxantrone (MTX) (in blue). (B, D, E and F) ABCG2 structure containing MTX in sequential docking analysis. (C) The overlay of A and B images. ABCG2 chains are light gray (A chain) and in dark grey (B chain). Amino acid residues that appear in the image are at a maximum of 4Å of distance.

4 DISCUSSION

Magnolol core structure and its structural isomer honokiol have been recently associated with a down-regulation of ABCG2 expression levels and ABCG2 inhibition [40]. Here, we screened 13 new magnolol derivatives to verify their potential as specific inhibitors of ABCG2 (Table 2). Unfortunately, the nature and the number of the substituents in the magnolol scaffold did not allow us to establish a precise structure activity relationship study. The best magnolol derivative was CT_M15, that is very similar to the precursor scaffold. The single difference of CT_M15 and the magnolol core structure was the replacement of the hydroxy group of magnolol by a methoxy group in the CT_M15.

Interestingly, the replacement of a second hydroxy group by other methoxy group in the CT_M16 enormously decreased the inhibition capacity (Table 2). The same behavior was observed replacing the two allyl groups (CT_M15) by two propyl groups (CT_M21). The insertion of a single hydroxy group (CT_M19 *versus* CT_M15) was enough to abrogate the inhibition effect. These data suggest an "all or nothing" logic, where a single chemical change is capable of completely modifying the behavior of a given structure. These findings are not commonly observed for other classes of ABCG2 inhibitors, such as chalcones [17], stilbenes [16], indeno[1,2-*b*]indoles [64] and chromones [15], where a single substitution shows a mild impact in the potential of inhibition.

In general, the presence of methoxy groups increase the ABCG2 inhibition effect [16,17]. We also observed this trend for some magnolol derivatives, once the replacement of hydroxy groups by methoxy groups increased the potency of ABCG2 inhibition: CT_M10 (two methoxy) > CT_M9 (one methoxy and one hydroxy) > CT_M7 (two hydroxy) (Table 2).

Between the two compounds that showed more than 50% of ABCG2 inhibition, CT_M15 stood out with the lower IC_{50} value and a non-cytotoxic profile. This promising compound showed an IC_{50} value of 9.5 µM when mitoxantrone was used as substrate. In addition, CT_M15 should be considered a complete inhibitor, since produced a saturation effect of inhibition at 100%, similarly to the reference inhibitor Ko143 (Fig. 1C). For ABCG2, many inhibitors are considered as partial inhibitors. Thus, the maximal inhibition effect is an important characteristic to be considered during the screening of new inhibitors [65]. Other desirable feature in the design of new ABC

inhibitors is the selectivity toward one single transporter [66,67]. Selectivity can reduce collateral effects due the interference on homeostasis processes and the pharmacokinetics of other drugs [68]. All magnolol derivatives were selective toward ABCG2 (Table 2), showing no inhibition of P-gp transport activity.

Magnolol and honokiol have been previously described as substrates of ABCG2 [40]. Here, the hypothesis of a transport mediated by ABCG2 was investigated by a cell viability assay using the parental and cells overexpressing ABCG2. Interestingly, both CT_M10 and CT_M15 were not transported by ABCG2 (Fig. 2A and B). Also, CT_M15 showed a very low cytotoxicity even in a long-term experiment employing high concentrations (more than 10-fold greater than the IC_{50} value) (Fig. 2B). The therapeutic ratio was stablished considering two important characteristics of these inhibitors: potency of inhibition (IC_{50} value) and cytotoxicity (IG_{50} value). With the lower IC_{50} value and a cytotoxicity estimated as >100 µM, CT_M15 showed a TR at least 6-fold higher than CT_M10. The TR observed for CT_M15 was similar to the porphyrin 4B, recently described as a new selective ABCG2 inhibitor [21], but very lower than the observed for chromone 6g (MBL-II-141), that shows one of the best TR (~2000) already described [15].

To better understand the mechanism of inhibition, membrane-based approaches were used to evaluate the effect of CT_M15 on ATPase activity and thermostability of ABCG2. The efflux of substrates mediated by ABC transporters through the cellular membrane depends on binding and hydrolysis of ATP [2] and, in general, functional inhibitors (compounds that inhibit the transport activity) also inhibit the ATPase activity, such as Ko143, a reference ABCG2 inhibitor [69]. However, differently of P-gp, it is not uncommon for ABCG2 that functional inhibitors stimulate the ATPase activity, such as stilbenes [16], tetrahydroquinoline/4,5-dihydroisoxazole molecular hybrids [70], indeno[1,2-b]indoles [20], Ulixertinib [71] and Rociletinib [72]. Here, we observed a rare and complex effect triggered by CT_M15, a dual behavior: stimulation at low concentrations and inhibition at high concentrations (Fig. 3A). Despite rare, this effect already was described for nilotinib and gefitinib [61,62]. The thermostability assay showed a decrease of protein stability in the presence of CT_M15 and ATP, since the IT_{50} decreased by approximately 10 °C. This result was similar to the observed for porphyrin 4B [21] and confirmed structural protein changes induced by CT_M15 binding (Fig. 3C).

Cell-based approaches were also employed to better understand the inhibition mechanism of CT_M15. Confocal microscopy allowed us to verify that this magnolol derivative was able to inhibit the ABCG2-mediated efflux of Hoechst 33342, similarly to Ko143 (Fig. 4A), and confirming that the ABCG2 inhibition caused by CT_M15 is independent of the substrate. To better understand the type of inhibition caused by CT_M15, a kinetic experiment was conducted. Using increasing concentrations of the inhibitor and mitoxantrone as substrate, CT_M15 showed a mixed type of inhibition (Fig. 4E). The same type of inhibition was recently observed for porphyrin 4B [21]. Another way to study the interaction of ligands on ABCG2 is by the 5D3 shift assay [65]. Generally, the binding of the conformation-sensitive antibody 5D3 on the extracellular loop of ABCG2 is increased by inhibitors, and not affected or even decreased by substrates [73–75]. CT_M15 showed the same behavior that functional inhibitors (Fig. 4C and D), confirming conformational changes due to CT_M15 binding.

It was found that CT_M15 bound to the region corresponding to site 2 of ABCG2, that corresponds to the entry of protein substrates [76], being close to important residues for the substrate expulsion movement, such as E446 [77]. In the case of CT_M16, the inactive analogue, there was no binding to the inner portion of the protein, a situation that could explain the lack of MTX transport inhibition provided by this compound. It is possible that the presence of the hydroxyl in CT_M15 and, consequently, a possible action as a hydrogen bond donor with other amino acid residues of the protein, has a relevant role for the observed inhibition. Although it is not possible to exclude the ability of CT_M16 to interact through water-mediated hydrogen bonds with its methoxy groups, the stabilization promoted is possibly inferior to that present in CT_M15, being insufficient for the molecule to be able to bind firmly to the transporter and sterically prevent and constrict the transmembrane helices of the central cavity, characteristic of the progression from the catalytic cycle to the substrate transport step [78].

In summary, the magnolol derivative CT_M15 is a promising complete ABCG2 inhibitor, that differently of the magnolol core structure does not affect the expression levels and is not transported by ABCG2 [40]. CT_M15 is selective toward ABCG2 and trigger allosteric effects, binding in a different site that substrates. Finally, the absence of cytotoxicity observed for CT_M15 become this inhibitor attractive for future pre-clinical studies.

5 REFERENCE

[1]   M.M. Gottesman, O. Lavi, M.D. Hall, J.P. Gillet, Toward a Better Understanding of the Complexity of Cancer Drug Resistance, Annu. Rev. Pharmacol. Toxicol. 56 (2016) 85–102. https://doi.org/10.1146/annurev-pharmtox-010715-103111.

[2]   R.W. Robey, K.M. Pluchino, M.D. Hall, A.T. Fojo, S.E. Bates, M.M. Gottesman, Revisiting the role of ABC transporters in multidrug-resistant cancer, Nat. Rev. Cancer. 18 (2018) 452–464. https://doi.org/10.1038/s41568-018-0005-8.

[3]   G. Szakács, A. Váradi, C. Özvegy-Laczka, B. Sarkadi, The role of ABC transporters in drug absorption, distribution, metabolism, excretion and toxicity (ADME-Tox), Drug Discov. Today. 13 (2008) 379–393. https://doi.org/10.1016/j.drudis.2007.12.010.

[4]   C.F. HIGGINS, Abc Transporters - From Microorganisms To Man, Annu. Rev. Cell Biol. 8 (1992) 67–113.

[5]   S.G. Aller, J. Yu, A. Ward, Y. Weng, S. Chittaboina, P.M. Harrell, Y.T. Trinh, Q. Zhang, I.L. Urbatsch, G. Chang, Structure of P-glycoprotein reveals a molecular basis for poly-specific drug binding, Science (80-.). 323 (2009) 1718–1722. https://doi.org/10.1126/science.1168750.Structure.

[6]   J.I. Fletcher, M. Haber, M.J. Henderson, M.D. Norris, ABC transporters in cancer: More than just drug efflux pumps, Nat. Rev. Cancer. 10 (2010) 147–156. https://doi.org/10.1038/nrc2789.

[7]   S.M. Stefan, Multi-target ABC transporter modulators: What next and where to go?, Future Med. Chem. 11 (2019) 2353–2358. https://doi.org/10.4155/fmc-2019-0185.

[8]   R.L. Juliano, V. Ling, A surface glycoprotein modulating drug permeability in Chinese hamster ovary cell mutants, BBA - Biomembr. 455 (1976) 152–162. https://doi.org/10.1016/0005-2736(76)90160-7.

[9]   A. Tamaki, C. Ierano, G. Szakacs, R.W. Robey, S.E. Bates, The controversial role of ABC transporters in clinical oncology., Essays Biochem. 50 (2011) 209–232. https://doi.org/10.1042/bse0500209.

[10]   E. Fox, S.E. Bates, Tariquidar (XR9576): A P-glycoprotein drug efflux pump inhibitor, Expert Rev. Anticancer Ther. 7 (2007) 447–459. https://doi.org/10.1586/14737140.7.4.447.

[11]   F.S. Chung, J.S. Santiago, M.F.M. De Jesus, C. V. Trinidad, M.F.E. See, Disrupting P-glycoprotein function in clinical settings: What can we learn from the fundamental aspects of this transporter?, Am. J. Cancer Res. 6 (2016) 1583–1598.

[12]   F. Morschhauser, P.L. Zinzani, M. Burgess, L. Sloots, F. Bouafia, C. Dumontet, Phase I/II trial of a P-glycoprotein inhibitor, Zosuquidar.3HCl trihydrochloride (LY335979), given orally in combination with the CHOP regimen in patients with non-Hodgkin's lymphoma, Leuk. Lymphoma. 48 (2007) 708–715. https://doi.org/10.1080/10428190701190169.

[13]   R. W. Robey, P. R. Massey, L. Amiri-Kordestani, S. E. Bates, ABC Transporters: Unvalidated Therapeutic Targets in Cancer and the CNS, Anticancer. Agents Med. Chem. 10 (2011) 625–633. https://doi.org/10.2174/187152010794473957.

[14] G. Valdameri, E. Genoux-Bastide, C. Gauthier, B. Peres, R. Terreux, S.M.B. Winnischofer, M.E.M. Rocha, A. DiPietro, A. Boumendjel, 6-Halogenochromones Bearing Tryptamine: One-Step Access to Potent and Highly Selective Inhibitors of Breast Cancer Resistance Protein, ChemMedChem. 7 (2012) 1177–1180. https://doi.org/10.1002/cmdc.201200154.

[15] G. Valdameri, E. Genoux, B. Peres, Substituted chromones as highly potent nontoxic inhibitors, specific for the breast cancer resistance protein., J. Med. Chem. 55 (2012) 3193–3200. https://doi.org/10.1021/jm2016528.Investigation.

[16] G. Valdameri, L. Pereira Rangel, C. Spatafora, J. Guitton, C. Gauthier, O. Arnaud, A. Ferreira-Pereira, P. Falson, S.M.B. Winnischofer, M.E.M. Rocha, C. Tringali, A. Di Pietro, Methoxy stilbenes as potent, specific, untransported, and noncytotoxic inhibitors of breast cancer resistance protein, ACS Chem. Biol. 7 (2012) 322–330. https://doi.org/10.1021/cb200435y.

[17] G. Valdameri, C. Gauthier, R. Terreux, R. Kachadourian, B.J. Day, S.M.B. Winnischofer, M.E.M. Rocha, V. Frachet, X. Ronot, A. Di Pietro, A. Boumendjel, Investigation of chalcones as selective inhibitors of the breast cancer resistance protein: Critical role of methoxylation in both inhibition potency and cytotoxicity, J. Med. Chem. 55 (2012) 3193–3200. https://doi.org/10.1021/jm2016528.

[18] G. Jabor Gozzi, A. Di Pietro, J. Guillon, G. Valdameri, C. Marminon, E. Winter, A. Nacereddine, A. Lacoudre, N. Daflon-Yunes, J. Jose, M. Le Borgne, S.M. Cadena, N. Pinaud, A. Bollacke, D. Aichele, Z. Bouaziz, W. Zeinyeh, Converting Potent Indeno[1,2- b]indole Inhibitors of Protein Kinase CK2 into Selective Inhibitors of the Breast Cancer Resistance Protein ABCG2, J. Med. Chem. 58 (2014) 265–277. https://doi.org/10.1021/jm500943z.

[19] G.J. Gozzi, Z. Bouaziz, E. Winter, N. Daflon-Yunes, M. Honorat, N. Guragossian, C. Marminon, G. Valdameri, A. Bollacke, J. Guillon, N. Pinaud, M. Marchivie, S.M. Cadena, J. Jose, M. Le Borgne, A. Di Pietro, Phenolic indeno[1,2-b]indoles as ABCG2-selective potent and non-toxic inhibitors stimulating basal ATPase activity, Drug Des. Devel. Ther. 9 (2015) 3481–3495. https://doi.org/10.2147/DDDT.S84982.

[20] D.H. Kita, N. Guragossian, I.F. Zattoni, V.R. Moure, F.G. de M. Rego, S. Lusvarghi, T. Moulenat, B. Belhani, G. Picheth, S. Bouacida, Z. Bouaziz, C. Marminon, M. Berredjem, J. Jose, M.B. Gonçalves, S. V. Ambudkar, G. Valdameri, M. Le Borgne, Mechanistic basis of breast cancer resistance protein inhibition by new indeno[1,2-b]indoles, Sci. Rep. 11 (2021) 1–16. https://doi.org/10.1038/s41598-020-79892-w.

[21] I.F. Zattoni, T. Kronenberger, D.H. Kita, L.D. Guanaes, M.M. Guimarães, L. de Oliveira Prado, M. Ziasch, L.C. Vesga, F. Gomes de Moraes Rego, G. Picheth, M.B. Gonçalves, M.D. Noseda, D.R.B. Ducatti, A. Poso, R.W. Robey, S. V. Ambudkar, V.R. Moure, A.G. Gonçalves, G. Valdameri, A new porphyrin as selective substrate-based inhibitor of breast cancer resistance protein (BCRP/ABCG2), Chem. Biol. Interact. 351 (2022). https://doi.org/10.1016/j.cbi.2021.109718.

[22] S. Zhang, X. Yang, M.E. Morris, Flavonoids are inhibitors of breast cancer resistance protein (ABCG2)-mediated transport., Mol. Pharmacol. 65 (2004) 1208–1216. https://doi.org/10.1124/mol.65.5.1208.

[23] C.J. Henrich, R.W. Robey, K. Takada, H.R. Bokesch, S.E. Bates, S. Shukla, S. V Ambudkar, J.B. Mcmahon, K.R. Gustafson, Botryllamides: Natural Product Inhibitors of ABCG2, ACS Chem. Biol. 4 (2009) 637–647.

[24] S. Shukla, H. Zaher, A. Hartz, B. Bauer, J.A. Ware, S. V. Ambudkar, Curcumin inhibits the activity of ABCG2/BCRP1, a multidrug resistance-linked ABC drug transporter in mice, Pharm. Res. 26 (2009) 480–487. https://doi.org/10.1007/s11095-008-9735-8.

[25] A. Sarrica, N. Kirika, M. Romeo, M. Salmona, L. Diomede, Safety and Toxicology of Magnolol and Honokiol, Planta Med. (2018). https://doi.org/10.1055/a-0642-1966.

[26] J.H. Chen, K.F. Ke, J.H. Lu, Y.H. Qiu, Y.P. Peng, Protection of TGF-β1 against neuroinflammation and neurodegeneration in Aβ1-42-induced alzheimer's disease model rats, PLoS One. 10 (2015) 1–19. https://doi.org/10.1371/journal.pone.0116549.

[27] M. Maioli, V. Basoli, P. Carta, D. Fabbri, M.A. Dettori, S. Cruciani, P.A. Serra, G. Delogu, Synthesis of magnolol and honokiol derivatives and their effect against hepatocarcinoma cells, PLoS One. 13 (2018) 1–21. https://doi.org/10.1371/journal.pone.0192178.

[28] J. Shen, H. Ma, T. Zhang, H. Liu, L. Yu, G. Li, H. Li, M. Hu, Magnolol Inhibits the Growth of Non-Small Cell Lung Cancer via Inhibiting Microtubule Polymerization, Cell. Physiol. Biochem. 42 (2017) 1789–1801. https://doi.org/10.1159/000479458.

[29] S. Chei, H.J. Oh, J.H. Song, Y.J. Seo, K. Lee, B.Y. Lee, Magnolol Suppresses TGF-β-Induced Epithelial-to-Mesenchymal Transition in Human Colorectal Cancer Cells, Front. Oncol. 9 (2019) 1–11. https://doi.org/10.3389/fonc.2019.00752.

[30] H. Chen, W. Fu, H. Chen, S. You, X. Liu, Y. Yang, Y. Wei, J. Huang, W. Rui, Magnolol attenuates the inflammation and enhances phagocytosis through the activation of MAPK, NF-κB signal pathways in vitro and in vivo, Mol. Immunol. 105 (2019) 96–106. https://doi.org/10.1016/j.molimm.2018.11.008.

[31] Y.C. Cheng, M.J. Tsao, C.Y. Chiu, P.C. Kan, Y. Chen, Magnolol inhibits human glioblastoma cell migration by regulating N-cadherin, J. Neuropathol. Exp. Neurol. 77 (2018) 426–436. https://doi.org/10.1093/jnen/nly021.

[32] A.M. Ranaware, K. Banik, V. Deshpande, G. Padmavathi, N.K. Roy, G. Sethi, L. Fan, A.P. Kumar, A.B. Kunnumakkara, Magnolol: A neolignan from the Magnolia family for the prevention and treatment of cancer, Int. J. Mol. Sci. 19 (2018) 1–21. https://doi.org/10.3390/ijms19082362.

[33] N. Li, Y. Song, W. Zhang, W. Wang, J. Chen, A.W. Wong, A. Roberts, Evaluation of the in vitro and in vivo genotoxicity of magnolia bark extract, Regul. Toxicol. Pharmacol. 49 (2007) 154–159. https://doi.org/10.1016/j.yrtph.2007.06.005.

[34] Z. Liu, X. Zhang, W. Cui, X. Zhang, N. Li, J. Chen, A.W. Wong, A. Roberts, Evaluation of short-term and subchronic toxicity of magnolia bark extract in rats, Regul. Toxicol. Pharmacol. 49 (2007) 160–171. https://doi.org/10.1016/j.yrtph.2007.06.006.

[35] Y.J. Lee, Y.M. Lee, C.K. Lee, J.K. Jung, S.B. Han, J.T. Hong, Therapeutic applications of compounds in the Magnolia family, Pharmacol. Ther. 130 (2011) 157–176. https://doi.org/10.1016/j.pharmthera.2011.01.010.

[36] M. Li, F. Zhang, X. Wang, X. Wu, B. Zhang, N. Zhang, W. Wu, Z. Wang, H. Weng, S. Liu, G. Gao, J. Mu, Y. Shu, R. Bao, Y. Cao, J. Lu, J. Gu, Y.

Liu, Magnolol inhibits growth of gallbladder cancer cells through the p53 pathway, Cancer Sci. 106 (2015) 1341–13501. https://doi.org/10.1111/cas.12762.

[37]   S. Di Micco, L. Pulvirenti, I. Bruno, S. Terracciano, A. Russo, M.C. Vaccaro, D. Ruggiero, V. Muccilli, N. Cardullo, C. Tringali, R. Riccio, G. Bifulco, Identification by Inverse Virtual Screening of magnolol-based scaffold as new tankyrase-2 inhibitors, Bioorganic Med. Chem. 26 (2018) 3953–3957. https://doi.org/10.1016/j.bmc.2018.06.019.

[38]   L. Pulvirenti, V. Muccilli, N. Cardullo, C. Spatafora, C. Tringali, Chemoenzymatic Synthesis and α-Glucosidase Inhibitory Activity of Dimeric Neolignans Inspired by Magnolol, J. Nat. Prod. 80 (2017) 1648–1657. https://doi.org/10.1021/acs.jnatprod.7b00250.

[39]   H.K. Han, L.T. Van Anh, Modulation of P-glycoprotein expression by honokiol, magnololand 4-O-methylhonokiol, the bioactive components of Magnolia officinalis, Anticancer Res. 32 (2012) 4445–4452. https://doi.org/32/10/4445 [pii].

[40]   C.P. Yu, P.Y. Li, S.Y. Chen, S.P. Lin, Y.C. Hou, Magnolol and honokiol inhibited the function and expression of BCRP with mechanism exploration, Molecules. 26 (2021) 1–10. https://doi.org/10.3390/molecules26237390.

[41]   R.W. Robey, Y. Honjo, K. Morisaki, T.A. Nadjem, S. Runge, M. Risbood, M.S. Poruchybsky, S.E. Bates, Mutations at amino-acid 482 in the ABCG2 gene affect substrate and antagonist specificity, Br. J. Cancer. 89 (2003) 1971–1978. https://doi.org/10.1038/sj.bjc.6601370.

[42]   C.O. Cardarelli, I. Aksentijevich, I. Pastan, M.M. Gottesman, Differential Effects of P-Glycoprotein Inhibitors on NIH3T3 Cells Transfected with Wild-Type (G185) or Mutant (V185) Multidrug Transporters, Cancer Res. 55 (1995) 1086–1091.

[43]   D.S. Heo, J.G. Park, K. Hata, R. Day, R.B. Herberman, T.L. Whiteside, EVALUATION OF TETRAZOLIUM-BASED SEMIAUTOMATIC COLORIMETRIC ASSAY FOR MEASUREMENT OF HUMAN ANTITUMOR CYTOTOXICITY, Cancer Res. 50 (1990) 3681–3690.

[44]   M.W. Pfaffl, A new mathematical model for relative quantification in real-time RT-PCR, Nucleic Acids Res. 29 (2001) 2003–2007. https://doi.org/10.1111/j.1365-2966.2012.21196.x.

[45]   S. Lemma, S. Avnet, M. Salerno, T. Chano, N. Baldini, Identification and validation of housekeeping genes for gene expression analysis of cancer stem cells, PLoS One. (2016). https://doi.org/10.1371/journal.pone.0149481.

[46]   F. Jacob, R. Guertler, S. Naim, S. Nixdorf, A. Fedier, N.F. Hacker, V. Heinzelmann-Schwarz, Careful Selection of Reference Genes Is Required for Reliable Performance of RT-qPCR in Human Normal and Cancer Cell Lines, PLoS One. (2013). https://doi.org/10.1371/journal.pone.0059180.

[47]   H. Ali, Z. Du, X. Li, Q. Yang, Y.C. Zhang, M. Wu, Y. Li, G. Zhang, Identification of suitable reference genes for gene expression studies using quantitative polymerase chain reaction in lung cancer in vitro, Mol. Med. Rep. (2015). https://doi.org/10.3892/mmr.2015.3159.

[48]   R.N. Sharan, S.T. Vaiphei, S. Nongrum, J. Keppen, M. Ksoo, Consensus reference gene(s) for gene expression studies in human cancers: end of the tunnel visible?, Cell. Oncol. (2015). https://doi.org/10.1007/s13402-015-0244-6.

[49]   C. Zhang, Y.Q. Wang, G. Jin, S. Wu, J. Cui, R.F. Wang, Selection of reference genes for gene expression studies in human bladder cancer using SYBR-green quantitative polymerase chain reaction, Oncol. Lett. (2017). https://doi.org/10.3892/ol.2017.7002.

[50]   D. Potashnikova, A. Gladkikh, I.A. Vorobjev, Selection of superior reference genes'combination for quantitative real-time PCR in B-cell lymphomas, Ann. Clin. Lab. Sci. (2015).

[51]   A.A. Saidova, D.M. Potashnikova, A. V. Tvorogova, I. V. Maly, W.A. Hofmann, I.A. Vorobjev, Specific and reliable detection of myosin 1c isoform a by RTqPCR in prostate cancer cells, PeerJ. (2018). https://doi.org/10.7717/peerj.5970.

[52]   S. V. Ambudkar, Drug-stimulatable ATPase activity in crude membranes of human MDR1- transfected mammalian cells, Methods Enzymol. 292 (1998) 504–514. https://doi.org/10.1016/S0076-6879(98)92039-0.

[53]   S. Lusvarghi, S. V Ambudkar, ATP-dependent thermostabilization of human P-glycoprotein (ABCB1) is blocked by modulators, Biochem. J. 476 (2019) 3737–3750. https://doi.org/10.1042/BCJ20190736.

[54]   J.J.P. Stewart, Optimization of parameters for semiempirical methods V: Modification of NDDO approximations and application to 70 elements, J. Mol. Model. 13 (2007) 1173–1213. https://doi.org/10.1007/s00894-007-0233-4.

[55]   O. Trott, A.J. Olson, Software News and Updates Gabedit — A Graphical User Interface for Computational Chemistry Softwares, J. Comput. Chem. 32 (2012) 174–182. https://doi.org/10.1002/jcc.

[56]   M.D. Hall, M.D. Handley, M.M. Gottesman, Is resistance useless? Multidrug resistance and collateral sensitivity, Trends Pharmacol. Sci. 30 (2009) 546–556. https://doi.org/10.1016/j.tips.2009.07.003.

[57]   J.D. Allen, A. van Loevezijn, J.M. Lakhai, M. van der Valk, O. van Tellingen, G. Reid, J.H.M. Schellens, G.-J. Koomen, A.H. Schinkel, Potent and specific inhibition of the breast cancer resistance protein multidrug transporter in vitro and in mouse intestine by a novel analogue of fumitremorgin C., Mol. Cancer Ther. 1 (2002) 417–25. http://www.ncbi.nlm.nih.gov/pubmed/12477054.

[58]   A. van Loevezijn, J.D. Allen, A.H. Schinkel, G.J. Koomen, Inhibition of BCRP-mediated drug efflux by fumitremorgin-type indolyl diketopiperazines., Bioorg. Med. Chem. Lett. 11 (2001) 29–32.

[59]   H. Glavinas, E. Kis, Á. Pál, R. Kovács, M. Jani, E. Vági, É. Molnár, S. Bánsághi, Z. Kele, T. Janáky, G. Báthori, O. Von Richter, G.J. Koomen, P. Krajcsi, ABCG2 (breast cancer resistance protein/mitoxantrone resistance-associated protein) ATPase assay: A useful tool to detect drug-transporter interactions, Drug Metab. Dispos. 35 (2007) 1533–1542. https://doi.org/10.1124/dmd.106.014605.

[60]   C. Özvegy, T. Litman, G. Szakács, Z. Nagy, S. Bates, A. Váradi, B. Sarkadi, Functional characterization of the human multidrug transporter, ABCG2, expressed in insect cells, Biochem. Biophys. Res. Commun. 285 (2001) 111–117. https://doi.org/10.1006/bbrc.2001.5130.

[61]   C. Hegedus, C. Özvegy-Laczka, A.Á. Apáti, M. Magócsi, K. Német, L. Orfi, G. Kéri, M. Katona, Z. Takáts, A. Váradi, G. Szakács, B. Sarkadi, Interaction of nilotinib, dasatinib and bosutinib with ABCB1 and ABCG2: Implications for altered anti-cancer effects and pharmacological properties, Br. J. Pharmacol. 158 (2009) 1153–1164. https://doi.org/10.1111/j.1476-5381.2009.00383.x.

[62]   N.B. Elkind, Z. Szentpetery, A. Apati, C. Ozvegy-Laczka, G. Varady, O.
         Ujhelly, K. Szabo, L. Homolya, A. Varadi, L. Buday, G. Keri, K. Nemet, B.
         Sarkadi, Multidrug transporter ABCG2 prevents tumor cell death induced by
         the epidermal growth factor receptor inhibitor Iressa (ZD1839, Gefitinib).,
         Cancer Res. 65 (2005) 1770–1777. https://doi.org/10.1158/0008-5472.CAN-
         04-3303.

[63]   G. Senisterra, I. Chau, M. Vedadi, Thermal denaturation assays in chemical
         biology, Assay Drug Dev. Technol. 10 (2012) 128–136.
         https://doi.org/10.1089/adt.2011.0390.

[64]   G.J. Gozzi, Z. Bouaziz, E. Winter, N. Daflon-Yunes, M. Honorat, N.
         Guragossian, C. Marminon, G. Valdameri, A. Bollacke, J. Guillon, N. Pinaud,
         M. Marchivie, S.M. Cadena, J. Jose, M. Le Borgne, A. Di Pietro, Phenolic
         indeno[1,2-b]indoles as ABCG2-selective potent and non-toxic inhibitors
         stimulating basal ATPase activity., Drug Des. Devel. Ther. 9 (2015) 3481–
         3495. https://doi.org/10.2147/DDDT.S84982.

[65]   I.F. Zattoni, L.C. Delabio, J. de P. Dutra, D.H. Kita, G. Scheiffer, M.
         Hembecker, G. da S. Pereira, V.R. Moure, G. Valdameri, Targeting breast
         cancer resistance protein (BCRP/ABCG2): Functional inhibitors and
         expression modulators., Eur. J. Med. Chem. 237 (2022) 114346.
         https://doi.org/10.1016/j.ejmech.2022.114346.

[66]   R.W. Robey, K.K.K. To, O. Polgar, M. Dohse, P. Fetsch, M. Dean, S.E.
         Bates, ABCG2: a perspective., Adv. Drug Deliv. Rev. 61 (2009) 3–13.
         https://doi.org/10.1016/j.addr.2008.11.003.

[67]   M.L.H. Vlaming, J.S. Lagas, A.H. Schinkel, Physiological and
         pharmacological roles of ABCG2 (BCRP): recent findings in Abcg2 knockout
         mice., Adv. Drug Deliv. Rev. 61 (2009) 14–25.
         https://doi.org/10.1016/j.addr.2008.08.007.

[68]   E. Teodori, S. Dei, C. Martelli, S. Scapecchi, F. Gualtieri, The Functions and
         Structure of ABC Transporters: Implications for the Design of New Inhibitors
         of Pgp and MRP1 to Control Multidrug Resistance (MDR), Curr. Drug
         Targets. 7 (2006) 893–909. https://doi.org/10.2174/138945006777709520.

[69]   L.D. Weidner, S.S. Zoghbi, S. Lu, S. Shukla, S. V. Ambudkar, V.W. Pike, J.
         Mulder, M.M. Gottesman, R.B. Innis, M.D. Hall, The Inhibitor Ko143 Is Not
         Specific for ABCG2, J. Pharmacol. Exp. Ther. 354 (2015) 384–393.
         https://doi.org/10.1124/jpet.115.225482.

[70]   L.C. Vesga, T. Kronenberger, A.K. Tonduru, D.H. Kita, I.F. Zattoni, C.C.
         Bernal, A.R.R. Bohórquez, S.C. Mendez-Sánchez, S. V. Ambudkar, G.
         Valdameri, A. Poso, Tetrahydroquinoline/4,5-Dihydroisoxazole Molecular
         Hybrids as Inhibitors of Breast Cancer Resistance Protein (BCRP/ABCG2),
         ChemMedChem. 16 (2021) 2686–2694.
         https://doi.org/10.1002/cmdc.202100188.

[71]   N. Ji, Y. Yang, Z.N. Lei, C.Y. Cai, J.Q. Wang, P. Gupta, X. Xian, D.H. Yang,
         D. Kong, Z.S. Chen, Ulixertinib (BVD-523) antagonizes ABCB1- and ABCG2-
         mediated chemotherapeutic drug resistance, Biochem. Pharmacol. 158
         (2018) 274–285. https://doi.org/10.1016/j.bcp.2018.10.028.

[72]   F. Zeng, F. Wang, Z. Zheng, Z. Chen, K.K. Wah To, H. Zhang, Q. Han, L. Fu,
         Rociletinib (CO-1686) enhanced the efficacy of chemotherapeutic agents in
         ABCG2-overexpressing cancer cells in vitro and in vivo, Acta Pharm. Sin. B.
         10 (2020) 799–811. https://doi.org/10.1016/j.apsb.2020.01.008.

[73]   Á. Telbisz, C. Hegedüs, C. Özvegy-Laczka, K. Goda, G. Várady, Z. Takáts, E. Szabó, B.P. Sorrentino, A. Váradi, B. Sarkadi, Antibody binding shift assay for rapid screening of drug interactions with the human ABCG2 multidrug transporter, Eur. J. Pharm. Sci. 45 (2012) 101–109. https://doi.org/10.1016/j.ejps.2011.10.021.

[74]   C. Özvegy-Laczka, G. Várady, G. Köblös, O. Ujhelly, J. Cervenak, J.D. Schuetz, B.P. Sorrentino, G.J. Koomen, A. Váradi, K. Német, B. Sarkadi, Function-dependent conformational changes of the ABCG2 multidrug transporter modify its interaction with a monoclonal antibody on the cell surface, J. Biol. Chem. 280 (2005) 4219–4227. https://doi.org/10.1074/jbc.M411338200.

[75]   C.J. Henrich, R.W. Robey, H.R. Bokesch, S.E. Bates, S. Shukla, S. V. Ambudkar, M. Dean, J.B. McMahon, New inhibitors of ABCG2 identified by high-throughput screening, Mol. Cancer Ther. 6 (2007) 3271–3278. https://doi.org/10.1158/1535-7163.MCT-07-0352.

[76]   T. Nagy, Á. Tóth, Á. Telbisz, B. Sarkadi, H. Tordai, A. Tordai, T. Hegedűs, The transport pathway in the {ABCG2} protein and its regulation revealed by molecular dynamics simulations, Cell. Mol. Life Sci. 78 (2021) 2329–2339. https://doi.org/10.1007/s00018-020-03651-3.

[77]   N. Khunweeraphong, T. Stockner, K. Kuchler, The structure of the human {ABC} transporter {ABCG2} reveals a novel mechanism for drug extrusion, Sci. Rep. 7 (2017) 13767. https://doi.org/10.1038/s41598-017-11794-w.

[78]   Q. Yu, D. Ni, J. Kowal, I. Manolaridis, S.M. Jackson, H. Stahlberg, K.P. Locher, Structures of {ABCG2} under turnover conditions reveal a key step in the drug transport mechanism, Nat. Commun. 12 (2021) 4376. https://doi.org/10.1038/s41467-021-24651-2.

CAPTHER 2 – AN IN-HOUSE-BUILT AND LIGHT-EMITTING-DIODE-BASED PHOTODYNAMIC THERAPY DEVICE FOR ENHANCING VERTEPORFIN CYTOTOXICITY IN A 2D CELL CULTURE MODEL

Isadora da Silva Zanzarini[1], Gustavo Barbosa[1], Larissa de Oliveira Prado[1], Ingrid Fatima Zattoni[1], Gustavo Da Paz[1], Ademir Luiz do Prado[2,3], Waldemar Volanski[2], Marcos Dinís Lavarda[3], Fabiane Gomes de Moraes Rego[2], Geraldo Picheth[2], Vivian Rotuno Moure[1], Glaucio Valdameri[1]

[1]Pharmaceutical Sciences Graduation Program, Laboratory of Cancer Drug Resistance, Federal University of Parana, Curitiba, Brazil
[2]Pharmaceutical Sciences Graduation Program, Federal University of Parana, Curitiba, Brazil
[3]Federal Institute of Parana, Curitiba, Brazil

Correspondence: G. Valdameri, Pharmaceutical Sciences Graduate Program, Laboratory of Cancer Drug Resistance, Federal University of Parana, Rua Prefeito Lothario Meissner, 632, Jardim Botânico, Curitiba, PR 80210-170, Brazil

1 INTRODUCTION

Among the most lethal noncommunicable diseases, cancer represents a global leading cause of premature death, accounting for nearly 10 million deaths in 2020, representing about one in six deaths worldwide[1]. Additionally, the multidrug resistance (MDR) phenomenon represents a tremendous public health threat as approved chemotherapeutic protocols fail to reach remission stages for that clinical condition[2]. Cancer cells can develop resistance to chemotherapy through several mechanisms; however, the overexpression of some ATP-binding cassette (ABC) transporters—ATP-dependent efflux pumps—is considered the main cause of MDR

development within a tumor microenvironment[3]. In addition to MDR, other cancer complications such as recurrence and metastasis reinforce the urgent demand to develop and improve therapeutic approaches to overcome this oncological challenge.

The curative utilization of light has been practiced for centuries[4], and PDT represents a clinically approved therapeutic approach for solid tumors. PDT combines the administration of a photosensitizer (PS) followed by light irradiation to generate ROS to exert selective cytotoxicity in tumor cells. This therapeutic approach is superior to conventional methods, including surgery, radiation, and chemotherapy[5]. It is a minimally invasive technique showing lower cytotoxicity in connective tissues[6]; the light application and PS accumulation directly in the tumor or its microenvironment ensure precise targeting and, consequently, minor undesirable systemic side effects[7] and possibility of repeated treatment at the same site. Moreover, the cost is lower than that of other approaches. Owing to its promising features, PDT can be considered an appropriate option for both single, especially in the case of inoperable tumors, or adjuvant cancer treatment[7] and represents an alternative for MDR related to chemotherapy[8,9].

The first report showing a high objective response rate using PDT was described in 1975 in mouse and rat model[10]. Since then, studies have been conducted using PDT with positive outcomes[7] both *in vivo* and *in vitro* with human tumor cell lines in 2D cell culture[11,12]. Considering the broad applicability of clinically approved PS, regardless of their specific accumulation pathways and wavelength ranges of absorption peaks, the general process is as follows: (i) PS uptake, (ii) peaking of PS concentration at the tumor or its microenvironment, (iii) light application, (iv) PS-light interaction, (v) transfer of PS excited-state energy to either tissue substrate or surrounding oxygen molecules, (vi) ROS production involving singlet oxygen or superoxide anion, (vii) tumor cells death via, essentially, necrosis or apoptosis (direct death), autophagy (cytoprotective mechanism), tissue ischemia (vascular damage), immune modulation, or an overlap of these mechanisms[7]. In this final stage, the activation of a specific cell death pathway depends on many factors such as cell characteristics, experimental design and, most importantly, PS intracellular localization and PDT-related targeted damage[13].

Verteporfin is a second-generation PS approved by regulatory agencies for clinical use in Norway and China to treat age-related macular degeneration[7]. After dose delivery, this prodrug was reported to partially accumulate in mitochondria[14] and induce cellular protein tyrosine phosphorylation and DNA fragmentation, leading to tumor cell apoptosis[15,16]. After 24 h incubation for verteporfin internalization, a PDT protocol using 690 nm wavelength setup is recommended to achieve effective levels of electromagnetic radiation transfer to adjacent molecules[7,17].

Regarding the light source for PDT, the classical diode laser systems are usually expensive, technically complicated, oversized, and thus unportable[18,19]. As a consequence of its single-wavelength profile, which can also be observed in LED-based PDT equipment, the demand for independent units for each photosensitizer application makes the utilization of diode laser systems even more complex and economically unfeasible[20,21]. Therefore, the utilization of LED machinery is considered the most promising alternative to solve not only costs[22] and maintenance issues but also to provide high power output and less harmful[23] and wider illuminating capability[24–27].

Despite the potential contribution that LED-based equipment can offer to PDT experiments[28], most commercial options still possess drawbacks such as lack of portability, high cost, and complex construction projects and operation[29]. The main objective of this work was to offer a simple and reliable tool for *in vitro* PDT assays. This paper describes PhotoACT, an in-house-built LED-based PDT device, which is inexpensive, user-friendly, and portable. As a proof of concept, this device is shown to enhance cytotoxicity of verteporfin in a 2D cell culture model and, therefore, can be used as a research tool in PDT experiments.

2 PROTOCOL

NOTE: See the **Table of Materials** for details related to all materials, reagents, and software used in this protocol.

2.1 DEVICE CONSTRUCTION

1. Saw 3 mm thickness medium-density fiberboards (MDF) to obtain pieces with dimensions shown in **Figure 1A**.

NOTE: Use the vector file (**Supplemental File 1**) for CNC cutting.

2. Build two boxes with the following dimensions (length x width x height (mm)): 330 x 235 x 225 and 300 x 220 x 150 for the bigger and smaller boxes, respectively (**Figure 1B**).

3. Drill the back of the bigger box to install a barrel jack connector. Drill the top of the bigger box, the top and bottom of the smaller box to provide a passage for electric cables (**Figure 1C**).

4. Paint all the internal surfaces with black ink to promote homogeneous light incidence (**Figure 1D**).

5. Attach, in parallel, three LED tapes with 10 LEDs each at the upper interior surface of the smaller box (**Figure 1E**).

6. Install a brightness sensor at the center of the bottom interior surface of the smaller box (**Figure 1F**).

7. Print the structure of the control unit (**Figure 1G**) using the 3D printing file (**Supplemental File 2**).

8. Install all the components (power button, potentiometers, time/start touchpad, LEDs, brightness sensor, LCD, buzzer, and power supply) at the ports of an ESP32 control board mounted at the control unit interior (**Figure 2**).

9. Upload the programming code (**Supplemental Files 3 - 5)** and run a test to check that all connections are working (**Figure 1H**).

10. Assemble the boxes and fix them together to avoid gaps and, consequently, external light interference and emitted light loss. Attach the

mounted control unit to the drilled area at the top of the prototype (**Figure 1I**).

11. Fix a front door of the same material and 330 x 225 (length x width (mm)) dimensions on the bigger box with two small hinges. Install a handle to manipulate the front door of the equipment. Also, attach velcro tapes sideways to the bigger box to reinforce the prototype closure (**Figure 1J**).

12. Attach four rubber foot pads at the bottom of the prototype to ensure more stability during the operations (**Figure 1K**).

2.2 CELL LINES: CULTIVATION, SEEDING, AND TREATMENT

2.2.1 Chemicals

1. Dissolve the porphyrin in dimethyl sulfoxide (DMSO) to achieve a concentration of 100 mM.

CAUTION: DMSO must be manipulated carefully (handling with the use of personal protective equipment and in a ventilated area). Manipulate both stock and diluted solutions carefully to avoid excessive light exposure.

2.2.2 Cell lines

1. Cultivate the HeLa cell line in Dulbecco's Modified Eagle's Medium (DMEM) low-glucose medium supplemented with 10% fetal bovine serum and 1% gentamicin.
2. Keep the culture flasks in a 5% CO_2 cell culture incubator at 37 °C.
3. Manage and inspect the cells until they reach 80%-90% confluence.

2.2.3 Seeding process

1. Remove the culture medium from the flask.
2. Wash the cell monolayer with PBS.
3. Detach the confluent cell culture with trypsin-EDTA (0.5%) 1x for 5 min at 37 °C. Stop the action of trypsin by resuspending the cells with culture medium supplemented with 10% fetal bovine serum and 1% gentamicin.

4. Count the resuspended cells with a hemocytometer and seed them into a 96-well plate at 2.0 × 104 cells/well.

5. Prepare two plates for dark and light conditions.

6. Incubate the plates for 24 h for cell attachment.

2.2.4 Treatment process

1. Remove the medium from both 96-well plates.

2. Treat the cells with 100 µL of increasing concentrations of verteporfin (0.045 to 24 µM, serial dilution).

3. Incubate the cells with drug treatment for 24 h to allow verteporfin internalization.

4. After 24 h, discard the medium containing the drug, wash the monolayer of cells with PBS (100 µL), and add drug-free medium (100 µL).

5. Cover one microplate with aluminum foil to protect it from light exposure and incubate it for 24 h. This plate will provide control data for PDT results (dark condition). The other microplate will be utilized on the light exposure condition in the device.

2.3 DEVICE OPERATION

1. Plug the PDT device into the electrical outlet and turn it on by pressing the power button.

2. Place the other microplate (light condition) into the PDT device and close the equipment by fastening the front door with the velcro tapes.

3. Use the potentiometers to adjust the RGB configuration (a RGB 255, 255, 255 experiment here) and set the color of light emission.

NOTE: Each RGB combination has a specific emission spectrum, which must be adjusted for experiments with different photosensitizers and, consequently, different absorbance curves.

4. Press the (+)/(-) touchpad to adjust the time configuration (a 60 min experiment here) and set the duration of the assay.

NOTE: The time configuration, in association with the irradiance value, will determine the fluence of the process-the light dose applied in the assay.

5. Check the setup information at the display.
6. Press the Start button to initiate the assay. Ensure that a one-beep buzzer is heard at the beginning of the assay.
7. In t''he course of the experiment, observe real-time information on the display, such as irradiance and time left.
8. Do not open the front door or change any configuration during the PDT assay.
9. At the end of the assay, wait for a four-beep buzzer and for the electronic system to turn all the LEDs off. Observe a Finished message and the final amount of energy expended-fluence-during the experiment in the display.

NOTE: The fluence final value is calculated using equation (1):

$$Fluence\ (F) = Irradiance\ (I) \times Time\ (s)$$

Where F equals to J/cm2 and I equals to mW/cm2 or mJ/s·cm2. The irradiance value considers the potency of the LEDs (emitting source) and the uniformly irradiated area of the dark chamber (660 cm2) (equation [2]):

$$Irradiance\ (I) = \frac{Potency}{Irradiated\ area}$$

The theorical irradiance value is shown on the device display throughout the entire PDT assay. At the end of the operation, use equation (3) to calculate the fluence:
Fluence (F) = irradiance (I, constant value) × operation time (s) (3)

2.4 CELL VIABILITY ASSAY

1. After the PDT assay, cover the microplate that was exposed to light and incubate for 24 h.

2. After the incubation period, remove the culture medium from both plates, wash the monolayer of cells with PBS (100 µL), and add MTT solution (0.5 mg/ml, 100 µL). Incubate both plates-dark and light conditions-for 4 h to allow formazan crystal formation.

3. Remove the MTT solution carefully and dissolve the purple crystals with a DMSO/ethanol (1:1) solution.

4. After complete dissolution of the crystals, carry out the absorbance measurement using a microplate reader at 595 nm.

NOTE: The device can be used in other important experiments such as ROS-mediated cell death triggered by photosensitizers after light exposure by flow cytometry[30].

3 REPRESENTATIVE RESULTS

The final PDT device, named the PhotoACT, included a dark chamber to allocate up to four multiwell microplates, with its upper interior surface equipped with a set of scattered LEDs programmed to emit distinct spectrums of visible light (**Figure 3** and **Supplemental File 6**). The device was built using two associated boxes: an internal box designed as a dark chamber for the PDT assays, and an external box to cover the internal chamber and hold the control unit (**Figure 1B**). The internal box was painted black (**Figure 1D**) and composed of a tape model of LED RGB WS2812 (or WS281B) with 30 LEDs and of 1 m length (which was later cut into three pieces) and 9 watts, which holds a built-in processor. This apparatus allowed a more controlled utilization and, consequently, more accurate color emission. The 30 LEDs were equally distributed over the entire upper interior surface of the PDT chamber by three parallel tapes with 10 LEDs each (**Figure 1E**). A homogeneous light incidence was established due to the low reflectivity of the black interior surfaces and the uniform distribution of LED configuration. A TSL2561 brightness sensor was also incorporated in the bottom center of the internal box to indicate the light incidence and serve as a quality control tool, guaranteeing irradiation uniformity inside the dark chamber (**Supplemental Table S1**) and monitoring the power of the LED system, which is known to have a certain number of hours of useful life (**Figure 1F**). The external box is a structure that covers the internal box, composed of six MDF parts, painted gray, and laser-cut for a perfect fit (**Figures 1A, B**). The control unit was designed using online software[31], 3D printed with polylactic acid as a single part using a 3D printer and painted gray. It holds all the

electronics components, including display, potentiometers, buttons, and a buzzer (**Figure 1I** and **Figure 2**).

To enable independent light incidence adjustments, the ESP32 controller board was selected to integrate the control unit (**Figure 2**). This configuration should allow a USB interface for programming, bluetooth, Wi-Fi, dual core processor, numerous ports, and the ability to communicate with I2C, a serial peripheral interface (SPI), and other interfaces. To operate the system, a program was written in C language through an integrated development environment (IDE). The code structure[32] is based on FreeRTOS, a free, real-time operational system supported by ESP32 controller board. The referred logic allows independent applications programming, which can be processed by ESP32 in echeloned or parallel approaches, making the project and its maintenance, improvement, and update processes much more versatile and secure.

The interface between the machine and the operator is user-friendly and consisted of a liquid crystal display (LCD), potentiometers, buttons, and a buzzer (**Figure 3 and Supplemental File 6**). The small, 16 mm x 2 mm (columns versus lines) LCD had a built-in HD44780 controller with inter-integrated circuit (I2C) communication protocol, which confers ease of installation and transmission versatility, respectively. The preliminary setup includes RGB and time adjustments by the operator. The light magnitude and color configuration can be adjusted using the potentiometers, which modify the intensity (0 to 255) of the three basic color components: RGB. These adjustments can result in several color compositions addressed in the international RGB colors table[33]. Each RGB composition owns a specific wavelength, which must be adjusted according to the PS used in the PDT experiment; the absorbance curve of the PS and the wavelength of the irradiation must be overlapped for the photoactivation to occur satisfactorily (**Supplemental Figure S1**). Along the process, the operation status with time left and light incidence information can be accessed on the LCD.

At the end of the programmed time, the electronics system turned all the LEDs off, emitted an audible warning, and showed on the display the total amount of energy per area (J/cm²), which was calculated by multiplying the constant value of irradiance by the operation time in seconds. This digital model presented a broad range of detection levels (limits between 0.1 and 40,000+ lux), an I2C interface, and a low intensity of electric current (0.5 mA and 15 µA in operation and standby status, respectively).

As a proof of concept, the device was used to enhance the cytotoxic effect of verteporfin in 2D HeLa cell culture after light exposure of 1 h (49.1 $\pm$ 0.6 J/cm^2). As shown in **Figure 4A**, the GI$_{50}$ value was 3.1 μM for the light condition and 13.8 μM for the dark condition. Thus, the shift of 4.4-fold comparing the conditions validated the use of verteporfin as a PS and the applicability of PhotoACT to PDT assays. To validate the use of the prototype described in this work, a commercial PDT device was used under the same experimental conditions, including PS, cells, and fluence, and the results compared. As shown in **Figure 4B**, both devices photoactivated verteporfin equally, enhancing the cytotoxic effect. These results confirmed the applicability of this in house-built PDT device (**Figure 4A,B**). Finally, the ROS-mediated cell death triggered by verteporfin after light exposure was confirmed by flow cytometry using DCFDA assay (**Figure 4C,D**).
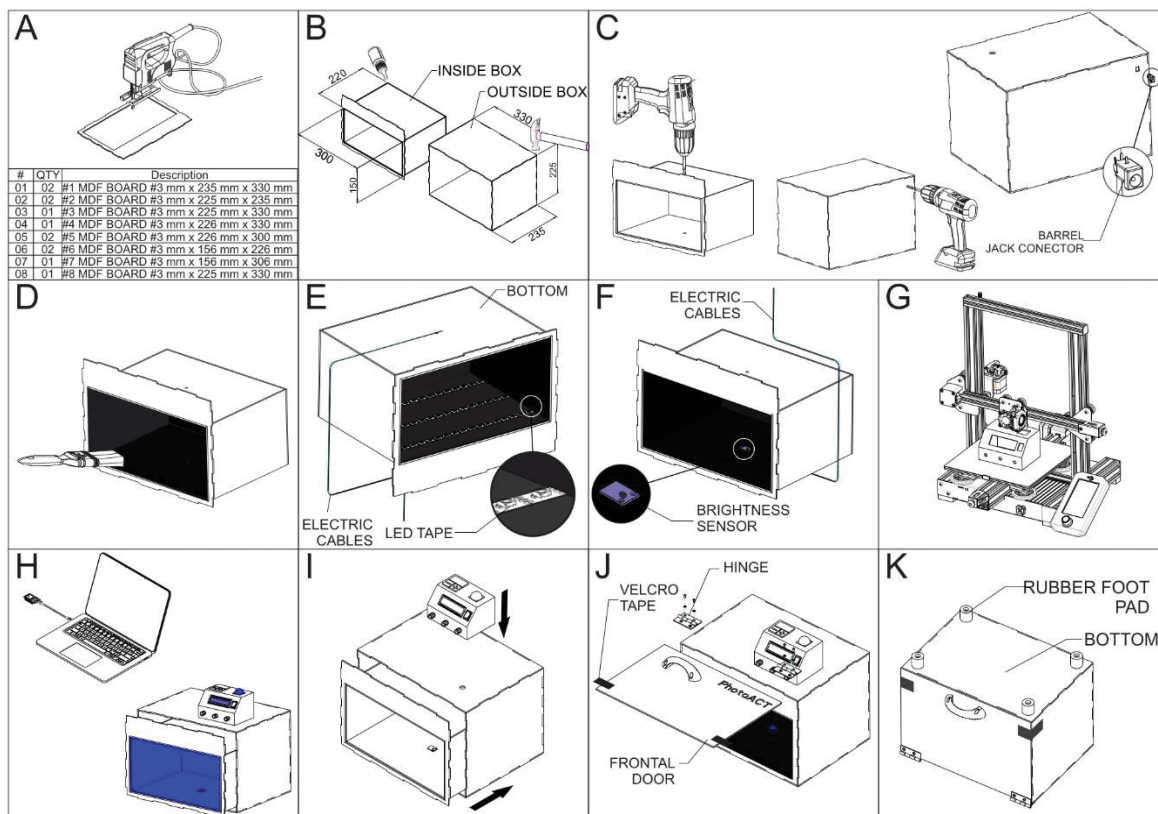
4 FIGURE AND TABLE LEGENDS:

Figure 1 - PhotoAct construction and assembly instructions. Detailed illustration of the construction, drilling, painting, mounting, and accessorizing components into the device. The panel shows a step-by-step guide to build the device.
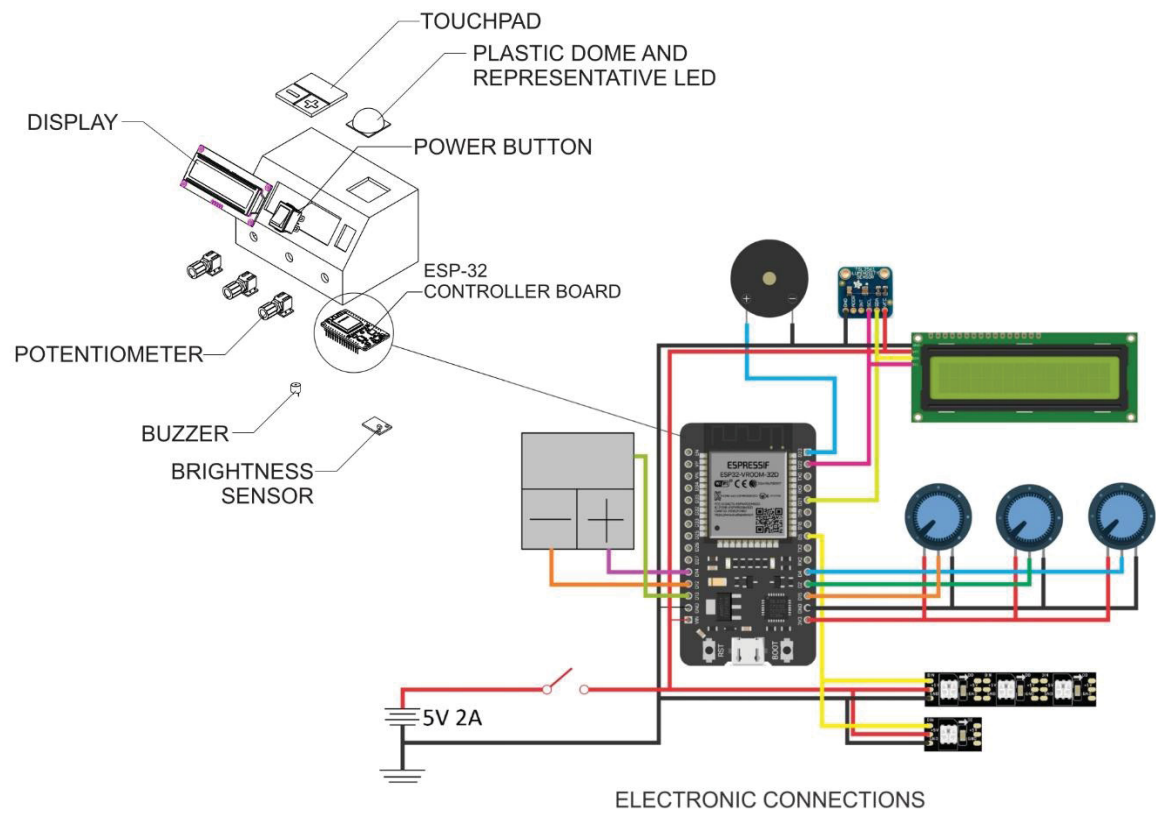
Figure 2 - The control unit construction and electronic installation instructions. Zoomed-in view drawing of exploded control unit and detailed scheme of electronic connections at ESP32 controller board ports with connections and components used in the prototype.
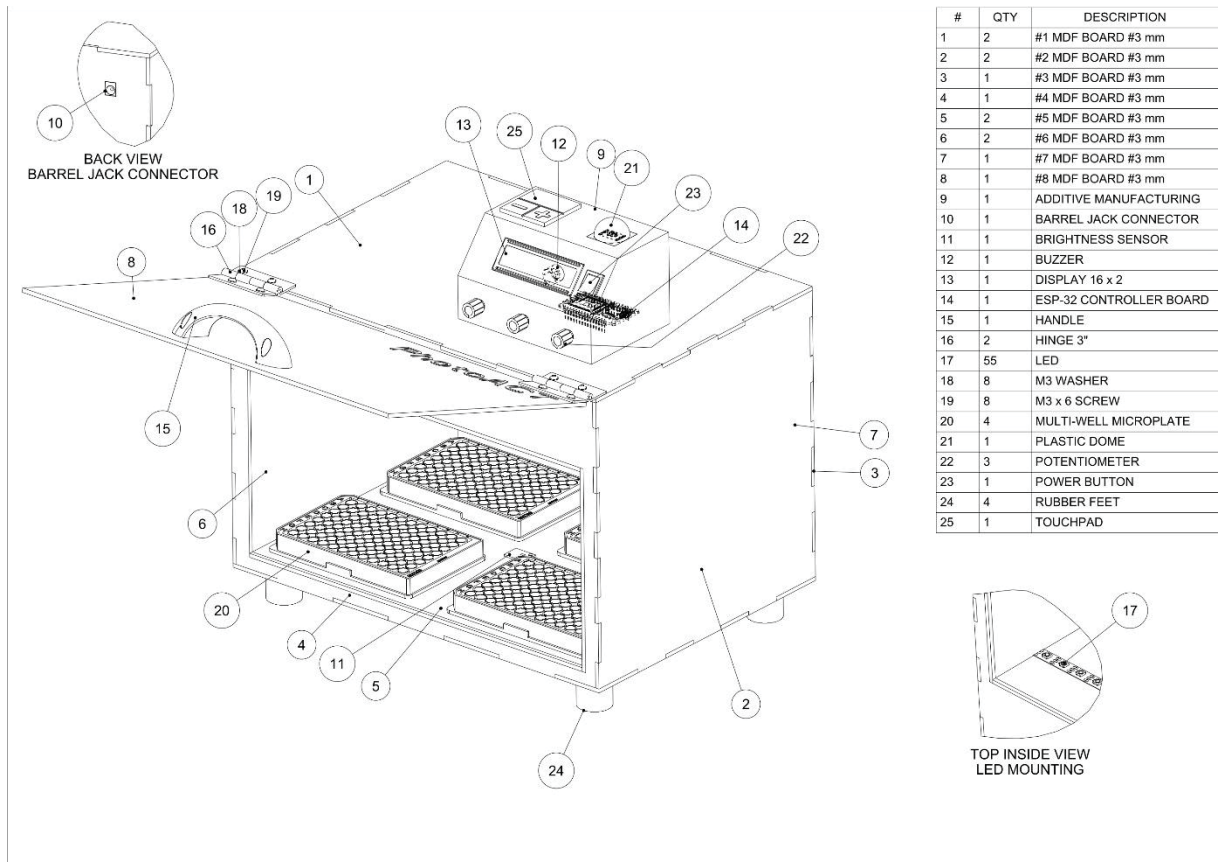
#	QTY	DESCRIPTION
1	2	#1 MDF BOARD #3 mm
2	2	#2 MDF BOARD #3 mm
3	1	#3 MDF BOARD #3 mm
4	1	#4 MDF BOARD #3 mm
5	2	#5 MDF BOARD #3 mm
6	2	#6 MDF BOARD #3 mm
7	1	#7 MDF BOARD #3 mm
8	1	#8 MDF BOARD #3 mm
9	1	ADDITIVE MANUFACTURING
10	1	BARREL JACK CONNECTOR
11	1	BRIGHTNESS SENSOR
12	1	BUZZER
13	1	DISPLAY 16 x 2
14	1	ESP-32 CONTROLLER BOARD
15	1	HANDLE
16	2	HINGE 3"
17	55	LED
18	8	M3 WASHER
19	8	M3 x 6 SCREW
20	4	MULTI-WELL MICROPLATE
21	1	PLASTIC DOME
22	3	POTENTIOMETER
23	1	POWER BUTTON
24	4	RUBBER FEET
25	1	TOUCHPAD

Figure 3 - Photoact representation. Assembly drawing of the final product design with bill of materials, labelling balloons, and detailed view of the upper interior LEDs. The figure allows to identify parts and components of the prototype.
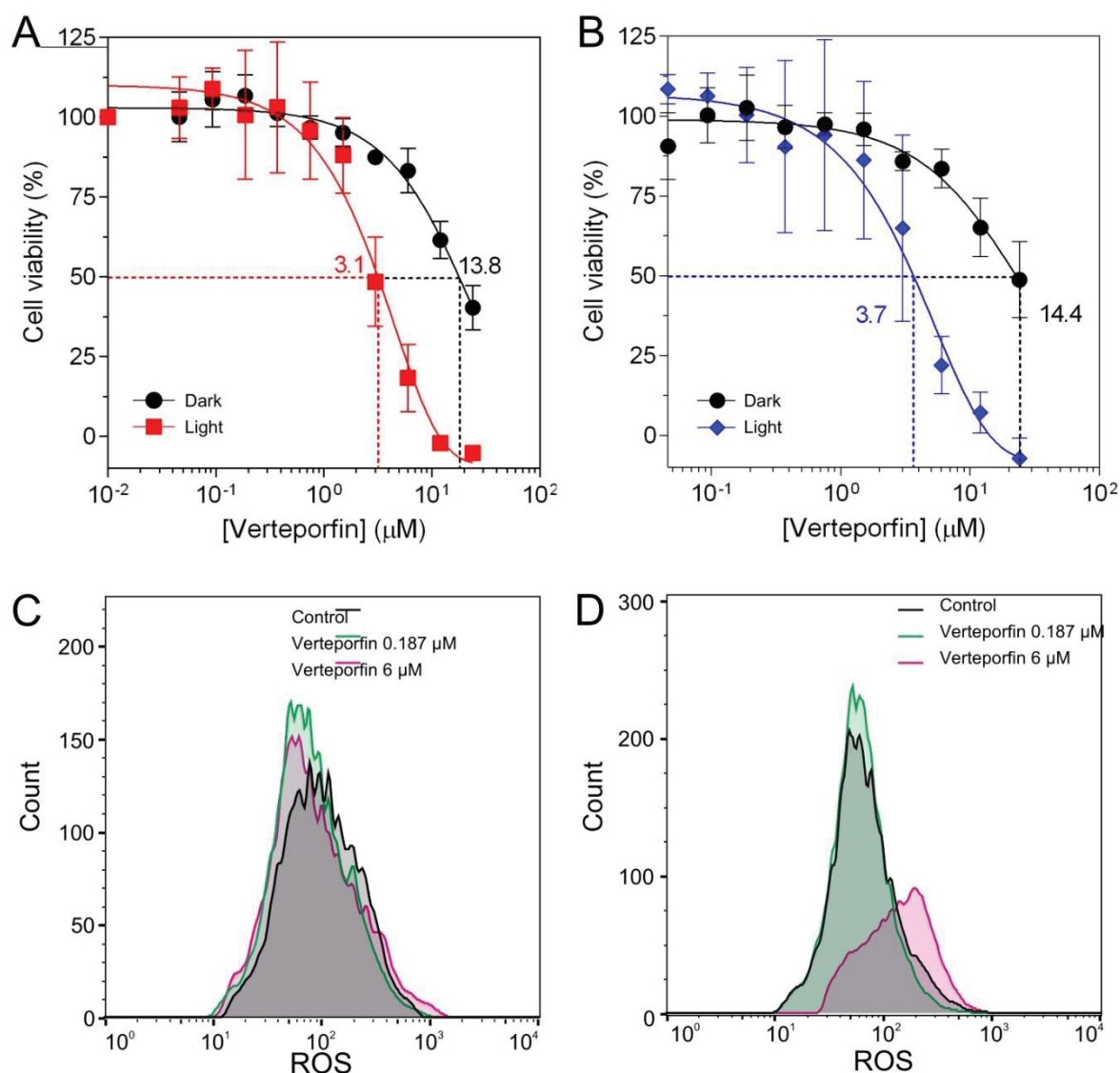
Figure 4 - In vitro phototoxicity of verteporfin and ROS generation (A,B). Cell viability assay performed using the MTT method: the assays were conducted to evaluate the cytotoxic profile of the photosensitizer verteporfin at different concentrations. HeLa cells were treated for 24 h with different concentrations of verteporfin (0.045-24 μM), exposed to light (PhotoACT (A) or commercial PDT equipment (B)) or dark conditions, and then subjected to the MTT assay. Both conditions showed a decreased cell viability at higher concentrations of verteporfin, but the light exposure-obtained from PDT assays-enhanced the cytotoxic profile of the PS, which implies that PDT enhances the cytotoxicity of verteporfin. The viability curves were fitted using GraphPad Prism 6 software. (C,D) HeLa cells were treated for 24 h with low and high concentrations of verteporfin (0.187 μM and 6 μM) and then exposed to light (PhotoACT) or dark conditions. Intracellular ROS levels were measured after irradiation by flow cytometry using DCFDA probe (incubation for 30 min at 1 μM). A right shift among the histograms implied higher fluorescence intensity because of a higher intracellular accumulation of DCF, and thus, greater ROS levels. The results showed no relevant difference in ROS levels in the dark condition (C) but showed a dose-response increase in ROS levels after verteporfin photoactivation (D). Abbreviations: ROS = reactive oxygen species; DCF = 2',7'-dichlorofluorescein; DCFDA = 2',7'-dichlorohydrofluorescein diacetate.
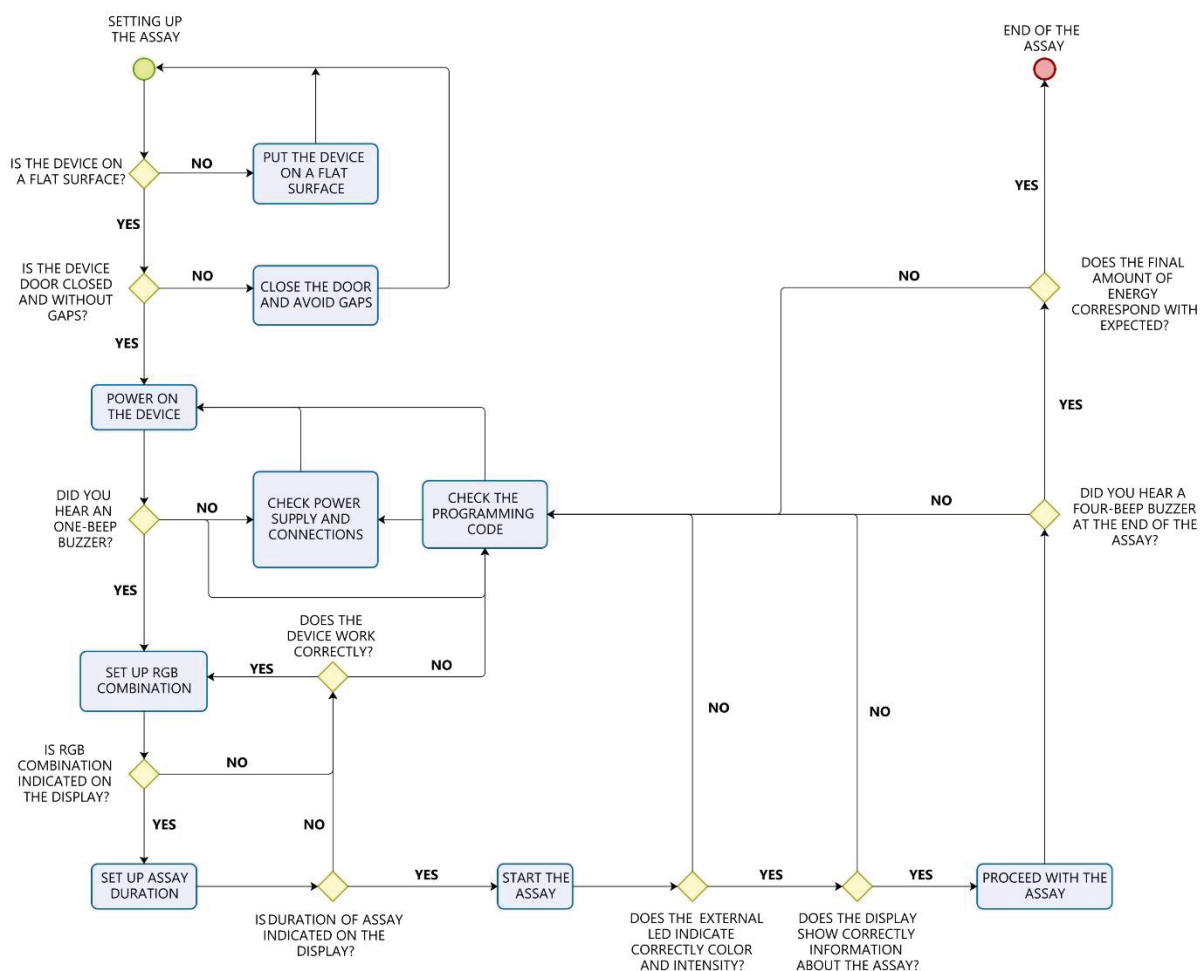
Figure 5 - The device's decision flowchart: preliminary setup and operation troubleshooting.

5 DISCUSSION

The final PhotoACT device was convenient to construct with commercially available, low-cost components at a total cost of less than $50. Additional advantages include low maintenance demands, capacity to irradiate multiple types of culture plates, the simultaneous use of up to 4 units per assay, weight (2 kg)/size (44 cm^3) that allow portability, accurate and reproducible irradiation (data not shown), and a user-friendly and simple setup interface that does not require connection to computers or other machines.

Certain critical steps of both construction and operation protocols gave rise to improvement opportunities during project conception. As a PDT chamber requires homogeneous light emission and consistent energy measurement, the internal and external boxes were sealed to avoid both exterior light interference and emitted light loss. Additional velcro tapes were fixed, sideways, on the frontal door to reinforce the chamber closure and ensure uninterrupted experiments. A representative LED was installed at the control unit to certify the required RGB configuration, indicating the color and intensity of the emitted light during the assay. Finally, the programming code underwent several upgrades to refine instant density measurements and final amounts of energy evaluations, endorsing reproducibility and mathematical consistency. Some other major details that require extra attention include: (i) homogeneous distribution of LEDs and central positioning of the brightness sensor to obtain representative and balanced results, (ii) installation of all components according to the electronic diagram (**Figure 2**) and programming code (**Supplemental Files 3 - 5**) to ensure correct operation, and (iii) the setup (keeping the same RGB and time configuration) before running an experiment to ensure consistent replicates with reliable results. Although the RGB system provides multiple visible color compositions with specific wavelengths, non-visible light experiments would require specific protocol upgrades. A decision flowchart is presented in **Figure 5** to provide a systematic problem-solving approach to find and correct problems or errors during the operation.

Designed to meet the demands of *in vitro* experimentation with validated results obtained with therapeutic activation of verteporfin to induce cytotoxicity in 2D HeLa cells (**Figure 4**), the PhotoACT can be recommended for universities, schools, industries, and other research centers. This device should extend the benefits of PDT

to scientific research exploring the mechanism of action of photosensitizers and their clinical applications.

6 REFERENCES

[1]   J. Ferlay, M. Ervik, F. Lam, M. Colombet, L. Mery, M. Piñeros, International Agency for Research on Cancer., Glob. Cancer Obs. Cancer Today. 23 (2021) 323–326. https://gco.iarc.fr/today/home (accessed May 11, 2022).

[2]   M.M. Gottesman, T. Fojo, S.E. Bates, Multidrug Resistance in Cancer: Role of Atp-Dependent Transporters, Nat. Rev. Cancer. 2 (2002) 48–58. https://doi.org/10.1038/nrc706.

[3]   G. Szakacs, J.K. Paterson, J.A. Ludwig, C. Booth-Genthe, M.M. Gottesman, G. Szakács, J.K. Paterson, J.A. Ludwig, C. Booth-Genthe, M.M. Gottesman, Targeting multidrug resistance in cancer, Nat. Rev. Drug Discov. 5 (2006) 219–234. https://doi.org/10.1038/nrd1984.

[4]   R. Ackroyd, C. Kelty, N. Brown, M. Reed, The History of Photodetection and Photodynamic Therapy¶, Photochem. Photobiol. 74 (2001) 656. https://doi.org/10.1562/0031-8655(2001)074<0656:thopap>2.0.co;2.

[5]   M.R. Hamblin, Photodynamic Therapy for Cancer: What's Past is Prologue, Photochem. Photobiol. 96 (2020) 506–516. https://doi.org/10.1111/php.13190.

[6]   H. Barr, C.J. Tralau, P.B. Boulos, A.J. MacRobert, R. Tilly, S.G. Bow, THE CONTRASTING MECHANISMS OF COLONIC COLLAGEN DAMAGE BETWEEN PHOTODYNAMIC THERAPY AND THERMAL INJURY, 46 (1987) 795–800.

[7]   J.F. Algorri, M. Ochoa, P. Roldán-Varona, L. Rodríguez-Cobo, J.M. López-Higuera, Photodynamic therapy: A compendium of latest reviews, Cancers (Basel). 13 (2021). https://doi.org/10.3390/cancers13174447.

[8]   E.C. Aniogo, B. Plackal, A. George, H. Abrahamse, The role of photodynamic therapy on multidrug resistant breast cancer, Cancer Cell Int. 19 (2019) 1–14. https://doi.org/10.1186/s12935-019-0815-0.

[9]   B.Q. Spring, I. Rizvi, N. Xu, T. Hasan, The Role of Photodynamic Therapy in Overcoming Cancer Drug Resistance., Photochem. Photobiol. Sci. (2015). https://doi.org/10.1039/C4PP00495G.

[10]   T.J. Dougherty, G.B. Grindey, R. Fiel, K.R. Weishaupt, D.G. Boyle, Photoradiation therapy. II. Cure of animal tumors with hematoporphyrin and

light, J. Natl. Cancer Inst. 55 (1975) 115–121. https://doi.org/10.1093/jnci/55.1.115.

[11]   M.E. Etcheverry, M.A. Pasquale, M. Garavaglia, Photodynamic therapy of HeLa cell cultures by using LED or laser sources, J. Photochem. Photobiol. B Biol. 160 (2016) 271–277. https://doi.org/10.1016/j.jphotobiol.2016.04.013.

[12]   Q. Guo, B. Dong, F. Nan, D. Guan, Y. Zhang, 5-Aminolevulinic acid photodynamic therapy in human cervical cancer via the activation of microRNA-143 and suppression of the Bcl-2/Bax signaling pathway, Mol. Med. Rep. 14 (2016) 544–550. https://doi.org/10.3892/mmr.2016.5248.

[13]   P. Mroz, A. Yaroslavsky, G.B. Kharkwal, M.R. Hamblin, Cell death pathways in photodynamic therapy of cancer, Cancers (Basel). 3 (2011) 2516–2539. https://doi.org/10.3390/cancers3022516.

[14]   S.M. Mahalingam, J.D. Ordaz, P.S. Low, Targeting of a Photosensitizer to the Mitochondrion Enhances the Potency of Photodynamic Therapy, ACS Omega. 3 (2018) 6066–6074. https://doi.org/10.1021/acsomega.8b00692.

[15]   D.J. Granville, J.G. Levy, D.W.C. Hunt, Photodynamic Treatment with Benzoporphyrin Derivative Monoacid Ring A Produces Protein Tyrosine Phosphorylation Events and DNA Fragmentation in Murine P815 Cells, Photochem. Photobiol. 67 (1998) 358–362.

[16]   A.P. Castano, T.N. Demidova, M.R. Hamblin, Mechanisms in photodynamic therapy: part two - cellular signaling, cell metabolism and modes of cell death, Photodiagnosis Photodyn. Ther. 2 (2014) 1–23. https://doi.org/10.1016/S1572-1000(05)00030-X.Mechanisms.

[17]   M.R. Detty, S.L. Gibson, S.J. Wagner, Current clinical and preclinical photosensitizers for use in photodynamic therapy, J. Med. Chem. 47 (2004) 3897–3915. https://doi.org/10.1021/jm040074b.

[18]   R.R. Allison, Photodynamic therapy: Oncologic horizons, Futur. Oncol. 10 (2014) 123–142. https://doi.org/10.2217/fon.13.176.

[19]   O. Chepurna, I. Shton, V. Kholin, V. Voytsehovich, V. Popov, S. Pavlov, N. Gamaleia, W. Wójcik, M. Zhassandykyzy, Photodynamic therapy with laser scanning mode of tumor irradiation, Opt. Fibers Their Appl. 2015. 9816 (2015) 98161F. https://doi.org/10.1117/12.2229030.

[20]   Z. Huang, A review of progress in clinical photodynamic therapy, Technol. Cancer Res. Treat. 4 (2005) 283–293. https://doi.org/10.1177/153303460500400308.

[21]   O. Chepurna, A. Grebinyk, Y. Petrushko, S. Prylutska, S. Grebinyk, V. Yashchuk, O. Matyshevska, U. Ritter, T. Dandekar, M. Frohme, J. Qu, T.Y. Ohulchanskyy, LED-based portable light source for photodynamic therapy, (2019) 45. https://doi.org/10.1117/12.2541774.

[22]   O. Hasson, A. Wishkerman, CultureLED: A 3D printer-based LED illumination cultivation system for multi-well culture plates, HardwareX. 12 (2022) e00323. https://doi.org/10.1016/j.ohx.2022.e00323.

[23]   X. Wu, J. Park, S.Y.A. Chow, M.C.Z. Kasuya, Y. Ikeuchi, B. Kim, Localised light delivery on melanoma cells using optical microneedles, Biomed. Opt. Express. 13 (2022) 1045. https://doi.org/10.1364/boe.450456.

[24]   A. Erkiert-Polguj, A. Halbina, I. Polak-Pacholczyk, H. Rotsztejn, Light-emitting diodes in photodynamic therapy in non-melanoma skin cancers - Own observations and literature review, J. Cosmet. Laser Ther. 18 (2016) 105–110. https://doi.org/10.3109/14764172.2015.1114635.

[25]   J. Neupane, S. Ghimire, S. Shakya, L. Chaudhary, V.P. Shrivastava, Effect of light emitting diodes in the photodynamic therapy of rheumatoid arthritis, Photodiagnosis Photodyn. Ther. 7 (2010) 44–49. https://doi.org/10.1016/j.pdpdt.2009.12.006.

[26]   E.C. Lins, C.F. Oliveira, O.C.C. Guimarães, C.A.D.S. Costa, C. Kurachi, V.S. Bagnato, A novel 785-nm laser diode-based system for standardization of cell culture irradiation, Photomed. Laser Surg. 31 (2013) 466–473. https://doi.org/10.1089/pho.2012.3310.

[27]   S.L. Hopkins, B. Siewert, S.H.C. Askes, P. Veldhuizen, R. Zwier, M. Heger, S. Bonnet, An: In vitro cell irradiation protocol for testing photopharmaceuticals and the effect of blue, green, and red light on human cancer cell lines, Photochem. Photobiol. Sci. 15 (2016) 644–653. https://doi.org/10.1039/c5pp00424a.

[28]   K. Zhang, M. Waguespack, E.M. Kercher, B.Q. Spring, An automated and stable LED array illumination system for multiwell plate cell culture photodynamic therapy experiments, Res. Sq. Preprint (2022) 1–18.

[29]   E.N. de Gálvez, J. Aguilera, P. Fonda-Pascual, M.V. de Gálvez, J.R. de Andrés-Díaz, S. Vidal-Asensi, E. Herrera-Acosta, A. Gago-Calderon, Analysis and evaluation of the operational characteristics of a new photodynamic therapy device, Photodiagnosis Photodyn. Ther. 37 (2022) 0–7. https://doi.org/10.1016/j.pdpdt.2022.102719.

[30]   L. Bretin, A. Pinon, S. Bouramtane, C. Ouk, L. Richard, M. Perrin, A. Chaunavel, C. Carrion, Photodynamic Therapy Activity of New Human Colorectal Cancer, Cancers (Basel). 11 (2019) 1–27.

[31]   T. Inc., SketchUp, (2022). https://www.sketchup.com/.

[32]   LCDR, PhotoDynamic Therapy (PDT) Equipment Repository, GitHub, Inc. (2022). https://github.com/PhotoDynamicTherapy.

[33]   W3C, CSS Color Module Level 3, W3C, Inc. (2022). https://www.w3.org/TR/css-color-3/#SRGB.

THESIS CONCLUSION

One of the goals of this thesis was the identification of new inhibitors of ABCG2 based on magnolol scaffold. Among a set of magnolol derivatives, **CT_M15** was the most promising, since completely and selectively inhibited ABCG2 activity. This compound was not transported by ABCG2 and positively showed minimal cytotoxicity. These results can guide *in vivo* experiments and the synthesis of a new generation of magnolol derivatives for improve some features, as the therapeutic ratio.

Other goal was the development of a simple, unexpensive and reproducible LED-based PDT device to conduct *in vitro* assays. The vast majority of Brazilian scientific production is generated by public universities, which operate with minimal governmental resources. The recent scientific movement of data sharing (open source) allows several minimally funded research groups to continue their research. Considering the importance of photodynamic therapy for MDR related to cancer studies and the fact that the equipment used to perform photodynamic therapy is known to be complex and expensive, our goal was to offer a solution for research groups that wish to pursue this important thematic area of science.

SUPPLEMENTARY DATA

CHAPTER 02 – AN IN-HOUSE-BUILT AND LIGHT-EMITTING-DIODE-BASED PHOTODYNAMIC THERAPY DEVICE FOR ENHANCING VERTEPORFIN CYTOTOXICITY IN A 2D CELL CULTURE MODEL
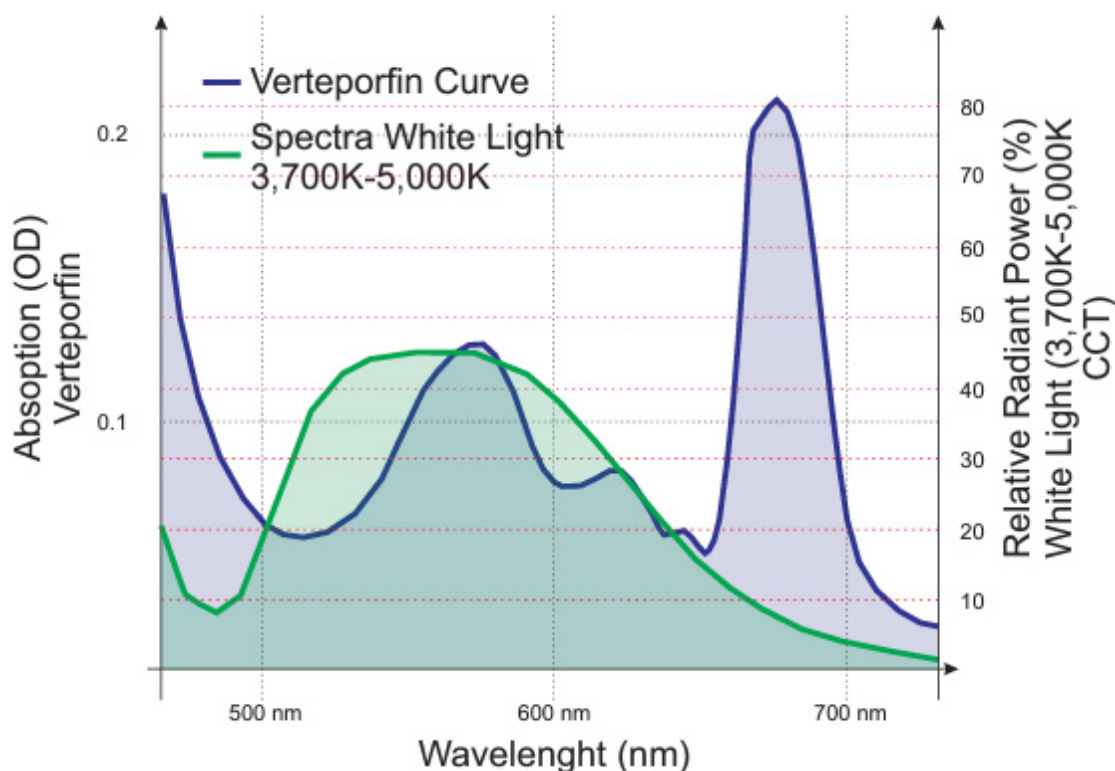
Supplemental Figure S1 - Overlap between the absorbance curve of verteporfin and the LED emission spectrum of the device. Absorption spectrum of verteporfin with its specific absorbance peaks (x,y') and LED emission spectrum of RGB 255, 255, 255-white color (3,700K-5,000K CCT) utilized to photoactivate the photosensitizer (x,y"). The overlap between the different absorbance peaks of verteporfin and the white irradiating light corroborates the photoactivation of the photosensitizer, which was also confirmed by the biological results.

SUPPLEMENTAL TABLE S1 - IRRADIATION UNIFORMITY TESTS

IRRADIATION UNIFORMITY TESTS	
Configuration: RGB 255, 255, 255	Time: 5 min
POSITION OF THE BRIGHTNESS SENSOR	**INSTANT LUMINOSITY (lumen)**
Bottom Right	23.79
Bottom Left	24.65
Center	24.04
Upper Left	25.44
Upper Right	23.88
MEAN ± SD	**24.36 ± 0.69**

Instant luminosity (lumen) measured by the brightness sensor at different points of the irradiated area. The presented results show no expressive variation, which attest the uniform irradiation of the device.